Analytical determination of non-local parameter value to investigate the axial buckling of nanoshells affected by the passing nanofluids and their velocities considering various modified cylindrical shell theories

Soheil Oveissi[1], Aazam Ghassemi[1,†], Mehdi Salehi[1], S. Ali Eftekhari[2], and Saeed Ziaei-Rad[3]

[1] *Department of Mechanical Engineering, Najafabad Branch, Islamic Azad University, Najafabad, Iran*
[2] *Department of Mechanical Engineering, Khomeinishahr Branch, Islamic Azad University, Khomeinishahr, Iran*
[3] *Department of Mechanical Engineering, Isfahan University of Technology, Isfahan* 84156-83111, *Iran*

(Received 23 June 2022; revised manuscript received 28 September 2022; accepted manuscript online 21 October 2022)

We analytically determine the nonlocal parameter value to achieve a more accurate axial-buckling response of carbon nanoshells conveying nanofluids. To this end, the four plates/shells' classical theories of Love, Flügge, Donnell, and Sanders are generalized using Eringen's nonlocal elasticity theory. By combining these theories in cylindrical coordinates, a modified motion equation is presented to investigate the buckling behavior of the nanofluid-nanostructure-interaction problem. Herein, in addition to the small-scale effect of the structure and the passing fluid on the critical buckling strain, we discuss the effects of nanoflow velocity, fluid density (nano-liquid/nano-gas), half-wave numbers, aspect ratio, and nanoshell flexural rigidity. The analytical approach is used to discretize and solve the obtained relations to study the mentioned cases.

Keywords: buckling, nonlocal cylindrical shell model, anofluid-nanostructure interaction, carbon nanotubes

PACS: 62.20.mq, 21.60.Cs, 61.46.–w, 47.60.–i **DOI:** 10.1088/1674-1056/ac9cba

1. Introduction

Plates and shells are the most widely used tools in industrial and manufacturing applications. With the advancement of technology, applications of these devices in various fields, especially in micro and nano scales of such as micro/nano-electromechanical systems,[1–5] nano-mechanical and biological sensors,[6,7] fluidic transfer devices in medical laboratories,[8,9] are indisputable. Therefore, the studies of mechanical behaviors such as bending,[10] buckling,[11] vibration,[12] and wave propagation,[13] have been highly regarded by researchers in various fields.

One of the materials that have recently received a lot of attention for their amazing properties and potential such as their mechanical, thermal, and electronic properties is the carbon nanotubes (CNTs) discovered by Iijima.[14] To study the mechanical properties, analyze the behavior, and model the carbon nano-shells and tubes, there are various classical and non-classical computational methods using continuum mechanics or laboratory methods and molecular dynamics simulations (MD). As the most well-known and widely used computational methods, which are much more cost-effective than molecular simulation, the models and theories of Euler–Bernoulli and Timoshenko for beams and Love, Flügge, Donnell, and Sanders for plates and shells can be declared that they produce acceptable results, especially in cylindrical coordinates.

On the other hand, one of the topics discussed for practical applications is the behavior of systems with nano-fluid-structural interaction such as fluid conveying CNTs.[15–18] Size, condition of nano-materials, and nature of atomic bonds can affect the properties of the materials and systems. So far, many studies have shown the inaccuracy of classical theories, and it has been proved that very small-scale structures have different mechanical behavior, and they are length-scale dependent parameters. Hence, with the help of non-classical theories such as nonlocal theory, surface stress theory, coupling stress, strain gradient, and so on the mentioned models are generalized so that the corresponding effects of the small-scale can also be considered for the structures. For example, Zhang *et al.* investigated the accuracy of the Euler Bernoulli beam and Donnell cylindrical shell models as well as their non-local counterparts in predicting the buckling strains of SWCNTs.[19] They revealed that the Euler–Bernoulli beam model with large aspect ratios is sufficient for predicting the buckling strains of CNTs. Silvestre *et al*. demonstrated that the Sanders cylindrical thin shell theory is completely suitable to model the CNTs buckling behavior with small aspect ratios.[20] They reported that the values of buckling strains and modes obtained by the cylindrical shell theory of Sanders have a close agreement with the MD simulations.

In the present work, by combining the four classical cylindrical shell theories and generalizing them for small scales

[†]Corresponding author. E-mail: aazam77@yahoo.com; a_ghassemi@pmc.iau.ac.ir
© 2023 Chinese Physical Society and IOP Publishing Ltd

using an applied non-classical theory, the buckling of carbon nanoshells (CNSs) that transfer various nanofluids with different velocities and densities is analytically investigated. Hence, based on the modified classical theories of Love, Flügge, Donnell, and Sanders, a governing equation is derived and presented for studying the nanofluid-nanostructure interaction problem. For this purpose, the small-scale effects of the structure and fluid are considered using the non-local parameter of Eringen's elasticity theory and Knudsen number, respectively. Using the obtained governing relations, it is shown how the value of the non-local parameter can be effective in achieving accurate results so that they are highly consistent with the simulation results of molecular dynamics. In other words, it is observed that the value of this parameter is a more important factor than the selected theory. Herein, in addition to the effects of the nanoscale size on the amount of critical buckling strain, we examine and discuss effects of fluid flow and its velocity, effect of the fluid flow density (nano-liquid/gas), effects of the longitudinal and circumferential half-wave numbers, the effects of the aspect ratio and flexural rigidity. To investigate the mentioned cases, the energy method and analytical approach are used to discretize and solve the obtained relationships.

2. Theoretical development

As shown in Fig. 1, a circular cylindrical shell with the mean radius r, thickness h, and length L is considered with a cylindrical coordinate system (x, θ, z). The origin point O is assumed to be at the center of a shell end. The longitudinal coordinate of this system is $x\varepsilon$ [0; L], circumferential coordinate is $\theta\varepsilon$ [0; 2π], and the radial is $z\varepsilon$ [$-h/2$; $h/2$]. In this system and intervals, the coordinates of displacement of an arbitrary point in the middle of the shell surface at the longitudinal, circumferential, and radial directions are represented by u, v, and w, respectively.

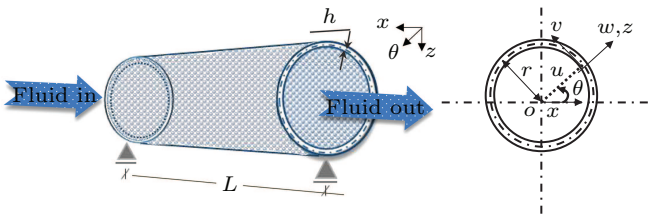


Fig. 1. A schematic illustration of a CNT shell structure and passing nanofluid with the coordinate system (x, θ, z) and displacement components (u, v, w).

In the following, in order to achieve the cylindrical displacement field equations, a set of basic field equations, namely, compatibility (displacement–strain), structural (strain–stress), and equilibrium (stress–force) equations are studied.

2.1. Compatibility equations

In this subsection, taking into account the coordinates of the cylindrical shell, the strain–displacement relations are presented using four classical theories of Love, Flügge, Donnell, and Sanders, respectively. All the four theories are based on the assumptions of the first Love's approximate theory. In other words, the basic assumptions related to the tiny deflection theory (classical theory) are expressed for thin, elastic, homogeneous, and isotropic plates that are based on the geometry of the deformation. By considering the strain components at a desired point in the shell, the compatibility equations concerning the cylindrical shell coordinates are generally given by

$$\begin{aligned}\varepsilon_{xx} &= \varepsilon^0_{xx} + zk_{xx},\\ \varepsilon_{\theta\theta} &= \varepsilon^0_{\theta\theta} + zk_{\theta\theta},\\ \varepsilon_{x\theta} &= \varepsilon^0_{x\theta} + zk_{x\theta},\end{aligned} \tag{1}$$

in which, according to the used theory, the strains and variations in the curvature of the middle surface are slightly different.

2.1.1. Love shell theory

The Love plate theory represents a two-dimensional mathematical model that is used to determine stresses and deformations in thin sheets under the influence of forces and moments. This theory is a generalization of the Euler–Bernoulli beam theory, which was proposed by Love[21] using the kinematics assumptions of Kirchhoff. Accordingly, based on the Love shell theory, the strain–displacement components of Eq. (1) are presented as follows:

$$\begin{aligned}&\left\{\varepsilon^0_{xx}, \varepsilon^0_{\theta\theta}, \gamma^0_{x\theta}\right\}\\ &= \left\{u_{,x},\ (1/r)[v_{,\theta} + w],\ v_{,x} + (1/r)u_{,\theta}\right\},\\ &\left\{k_{xx}, k_{\theta\theta}, k_{x\theta}\right\}\\ &= \left\{-w_{,xx},\ (1/r^2)[v_{,\theta} - w_{,\theta\theta}],\ (1/r)[v_{,x} - 2w_{,x\theta}]\right\}.\end{aligned} \tag{2}$$

2.1.2. Flügge shell theory

In this membrane theory of shells, the mechanical properties of thin and short shells are defined so that torsion and small bending moments can be neglected. This unusual simplification in the theory of shells makes it possible to examine different types of geometric shapes and supports, especially the shells of tanks and shell roofs. However, there are a lot of negative effects for this simplification and some defects appear during the review of problem-solving, this theory is more than a first-order approximation. If a shell is constructed and stored to withstand loaded stresses in the membrane, a desirable solution to the design problem in cases such as thin, light, and shell straightness can be the use of this theory.[22] Compatibility equations in this theory are defined as the following

relationships:

$$\begin{aligned}&\{\varepsilon^0_{xx},\varepsilon^0_{\theta\theta},\gamma^0_{x\theta}\}\\ &=\{u_{,x},\ (1/r)[v_{,\theta}+w],\ v_{,x}+(1/r)u_{,\theta}\},\\ &\{k_{xx},k_{\theta\theta},k_{x\theta}\}\\ &=\{-w_{,xx},\ (1/r^2)[-w-w_{,\theta\theta}],\ (1/r)\\ &\times[v_{,x}-w_{,x\theta}-(u_{,\theta}/2r)]\}.\end{aligned}\tag{3}$$

It should be noted that, unlike other theorems that strain-displacement relations are linear functions of thickness along the z-direction, these relations are not linear in Flügge theory, therefore the expression $(1+z/r)$ is used, instead of the $[(1=z/r)\approx 1]$ approximation.

2.1.3. Donnell and Sanders shell theories

These theories are very much considered due to the simplicity and accuracy of their application, and so far many researchers have used these theories to derive the governing equations for various problems. The disadvantage of the Donnell theory is that the resulting responses are reliable only in the range of very thin shells due to the inertial effects of inertia, in-plane stresses, and the effect of the shear modification.[23] Sanders[24] managed to overcome the problem of instability in previous theories using the principle of virtual work. The strain-displacement relations are defined based on these shell theories as follows:[20]

$$\begin{aligned}\{\varepsilon^0_{xx},\varepsilon^0_{\theta\theta},\gamma^0_{x\theta}\}&=\{u_{,x}+(1/2)(w_{,x})^2+(1/2)\beta_z^2,\ (1/r)[v_{,\theta}+w]+(1/2)\beta_x^2+(1/2)\beta_z^2,v_{,x}+(1/r)u_{,\theta}-w_{,x}\beta_x\},\\ \{k_{xx},k_{\theta\theta},k_{x\theta}\}&=\{-w_{,xx},\ (1/r)\beta_{x,\theta},\ [(-w_{,x\theta}/r)+\beta_{x,\theta}+(\beta_z/r)]\},\end{aligned}\tag{4}$$

where

$$\begin{array}{ll}\beta_x=-w_{,\theta}/r,\quad \beta_z=0, & \text{for Donnell theory,}\\ \beta_x=(1/r)[v-w_{,\theta}],\quad \beta_z=(1/2)[v_{,x}-(u_{,\theta}/r)], & \text{for Sanders theory.}\end{array}\tag{5}$$

With the definition of z (in Eq. (1)) as the distance of an arbitrary point of shell from the middle surface, β_x and β_z are the rotation in the perpendicular direction to the $r\theta z$ plane (around the x-axis), and the rotation in the perpendicular direction to the $r\theta x$ plane (around the z-axis) respectively, so that the rotation z is orthogonal relative to the mid-surface. These two parameters play a key role in determining the results. Compared to Donnell's theory, the major drawback of Sanders's theory is the complexity of the final governing equations. To simplify these equations and the ability to duplicate them, the β_z value is considered to equal zero.

In order to provide a comprehensive compatibility relationship that includes all these four main and most popular theories, Eq. (1) is rewritten as

$$\begin{aligned}\varepsilon_{xx}&=u_{,x}+\frac{\alpha_1}{2}(w_{,x})^2+\frac{\alpha_2}{8}\left(v_{,x}-\frac{u_{,\theta}}{r}\right)^2-zw_{,xx},\\ \varepsilon_{\theta\theta}&=\frac{v_{,\theta}+w}{r}+\frac{\alpha_1}{2}\left(\frac{\alpha_2 v}{r}-\frac{w_{,\theta}}{r}\right)^2+\frac{\alpha_2}{8}\left(v_{,x}-\frac{u_{,\theta}}{r}\right)^2\\ &\quad+z\left[\frac{1}{r^2}(\alpha_3 v_{,\theta}-\alpha_4 w-w_{,\theta\theta})\right],\\ \gamma_{x\theta}&=\frac{u_{,\theta}}{r}+v_{,x}-\alpha_1 w_{,x}\left(\frac{\alpha_2 v}{r}-\frac{w_{,\theta}}{r}\right)\\ &\quad+z\left[\frac{1}{r}\left(-w_{,x\theta}+\alpha_5 v_{,x}-\frac{\alpha_6 u_{,\theta}}{r}\right)\right].\end{aligned}\tag{6}$$

The unknown coefficients of the above relations are presented in Table 1 so that the compatibility equations of each theory can be achieved by putting them in Eq. (6).

Table 1. Unknown coefficients of compatibility equations based on the Love, Flügge, Donnell, and Sanders theories.

Unknown coefficients	Shell theories			
	Love	Flügge	Donnell	Sanders
α_1	0	0	1	1
α_2	0	0	0	1
α_3	1	0	0	1
α_4	0	1	0	0
α_5	1	1	0	3/2
α_6	0	1	0	1/2

2.2. Constitutive equations

The constitutive equations (stress–strain relations) depend on the structure material. Based on the classical theory of thin plates and shells in which the transverse tension is not taken into account, the stress–strain relations are in-plane stress (one dimension is much smaller than the other two dimensions) for an elastic, homogeneous, and isotropic material and is defined as follows:[25]

$$\begin{bmatrix}\sigma_{xx}\\ \sigma_{\theta\theta}\\ \sigma_{x\theta}\end{bmatrix}=\frac{E}{1-\nu^2}\begin{bmatrix}1 & \nu & 0\\ \nu & 1 & 0\\ 0 & 0 & 1-\nu\end{bmatrix}\begin{bmatrix}\varepsilon_{xx}\\ \varepsilon_{\theta\theta}\\ \varepsilon_{x\theta}\end{bmatrix},\tag{7}$$

where E and ν are Young's modulus and Poisson's ratio, respectively. It is obvious that a nanoscale structure, such as a carbon nanotube, is very thin in the z-direction, so there may be a small change in the stress components along its thickness. Therefore, of the plate, it can be deduced that other non-zero components will have a slight change over z for in-plain stress state. This conclusion can be summed up by considering the

cylindrical coordinates:

$$\sigma_x = \sigma_x(x,\theta), \quad \sigma_\theta = \sigma_\theta(x,\theta),$$
$$\tau_{x\theta} = \tau_{x\theta}(x,\theta), \quad \sigma_z = \tau_{xz} = \tau_{\theta z} = 0. \tag{8}$$

An important issue for obtaining more realistic results is the consideration of the nano-scale for the structure and the effect of size in the governing equations. As stated earlier, nanostructures will behave differently from macrostructure behavior due to the size-scale and other effective factors such as surface stress, strain gradients, and nonlocal effects of stress. In order to consider such effects, one can use nonclassical theories such as Eringen's nonlocal theory and generalize the governing equations. One of the reasons for using Eringen theory in this study, as well as the widespread use of other researchers, is the close and consistent agreement of the obtained results to the results of molecular dynamics simulations.[26] Thus, in accordance to this theory, Hooke's law for stress and strain relations in cylindrical coordinates are given as follows:[27]

$$\begin{Bmatrix} \sigma_{xx} \\ \sigma_{\theta\theta} \\ \sigma_{x\theta} \\ \sigma_{\theta x} \end{Bmatrix} - (e_0 a)^2 \nabla^2 \begin{Bmatrix} \sigma_{xx} \\ \sigma_{\theta\theta} \\ \sigma_{\theta x} \\ \sigma_{x\theta} \end{Bmatrix} = \begin{bmatrix} Q_{11} & Q_{12} & Q_{13} & Q_{14} \\ Q_{21} & Q_{22} & Q_{23} & Q_{24} \\ Q_{31} & Q_{32} & Q_{33} & Q_{34} \\ Q_{41} & Q_{42} & Q_{43} & Q_{44} \end{bmatrix} \begin{Bmatrix} \varepsilon_{xx} \\ \varepsilon_{\theta\theta} \\ \varepsilon_{x\theta} \\ \varepsilon_{\theta x} \end{Bmatrix}, \tag{9}$$

where $Q_{13} = Q_{31} = E/(1-\nu^2)$, $Q_{12} = Q_{21} = \nu E/(1-\nu^2)$, $Q_{33} = Q_{44} = E/2(1+\nu)$, $Q_{13} = Q_{31} = Q_{23} = Q_{32} = 0$, $Q_{14} = Q_{41} = Q_{24} = Q_{42} = 0$, and $Q_{34} = Q_{43} = 0$.

In addition, due to the considered geometry at cylindrical coordinates (Fig. 1), the Laplacian operator is defined as a simplified state of $\nabla^2 = \frac{\partial^2}{\partial x^2} + \frac{1}{r^2}\frac{\partial^2}{\partial \theta^2}$.

2.3. Equilibrium equations

The static equilibrium equations, i.e., the relationships between the forces and internal moments/stresses which are defined as resulting stress and coupling, are presented as follows:

$$(N_{xx}, N_{\theta\theta}, N_{x\theta}, N_{\theta x}) = \int_{-h/2}^{h/2} (\sigma_{xx}(1+\alpha_4 z/r), \sigma_{\theta\theta}, \sigma_{x\theta}(1+\alpha_4 z/r), \sigma_{\theta x})\,\mathrm{d}z,$$

$$(M_{xx}, M_{\theta\theta}, M_{x\theta}, M_{\theta x}) = \int_{-h/2}^{h/2} (\sigma_{xx}(1+\alpha_4 z/r), \sigma_{\theta\theta}, \sigma_{x\theta}(1+\alpha_4 z/r), \sigma_{\theta x}) z\,\mathrm{d}z. \tag{10}$$

In the above relations, the value of α_4 is presented in Table 1 for various theories. As mentioned above, it should be noted that the difference between the theory of flügge and other theories is that the strain-displacement relations are not linear functions along the z-direction. Hence, it is observed that $N_{x\theta}$ and $M_{x\theta}$ are not equal to $N_{\theta x}$ and $M_{\theta x}$, respectively. Applying Eringen's nonlinear theory and in accordance with Eqs. (9), we can rewrite Eqs. (10) as

$$N_{xx} - (e_0 a)^2 \nabla^2 N_{xx} = \int_{-h/2}^{h/2} \sigma_{xx}(1+\alpha_4 z/r)\,\mathrm{d}z, \tag{11a}$$
$$N_{\theta\theta} - (e_0 a)^2 \nabla^2 N_{\theta\theta} = \int_{-h/2}^{h/2} \sigma_{\theta\theta}\,\mathrm{d}z, \tag{11b}$$
$$N_{x\theta} - (e_0 a)^2 \nabla^2 N_{x\theta} = \int_{-h/2}^{h/2} \sigma_{x\theta}(1+\alpha_4 z/r)\,\mathrm{d}z, \tag{11c}$$
$$N_{\theta x} - (e_0 a)^2 \nabla^2 N_{\theta x} = \int_{-h/2}^{h/2} \sigma_{\theta x}\,\mathrm{d}z, \tag{11d}$$
$$M_{xx} - (e_0 a)^2 \nabla^2 M_{xx} = \int_{-h/2}^{h/2} \sigma_{xx} z(1+\alpha_4 z/r)\,\mathrm{d}z, \tag{11e}$$
$$M_{\theta\theta} - (e_0 a)^2 \nabla^2 M_{\theta\theta} = \int_{-h/2}^{h/2} \sigma_{\theta\theta} z\,\mathrm{d}z, \tag{11f}$$
$$M_{x\theta} - (e_0 a)^2 \nabla^2 M_{x\theta} = \int_{-h/2}^{h/2} \sigma_{x\theta} z(1+\alpha_4 z/r)\,\mathrm{d}z,$$
$$M_{\theta x} - (e_0 a)^2 \nabla^2 M_{\theta x} = \int_{-h/2}^{h/2} \sigma_{\theta x} z\,\mathrm{d}z. \tag{11g}$$

Substituting the constitutive equations, Eqs. (9), into Eqs. (11) and introducing the following parameters,

$$A_{ij} = \int_{-h/2}^{h/2} Q_{ij}\,\mathrm{d}z = Q_{ij} h, \quad B_{ij} = \int_{-h/2}^{h/2} z Q_{ij}\,\mathrm{d}z = 0,$$
$$C_{ij} = \int_{-h/2}^{h/2} z^2 Q_{ij}\,\mathrm{d}z = Q_{ij}\frac{h^3}{12}, \quad D_{ij} = \int_{-h/2}^{h/2} z^3 Q_{ij}\,\mathrm{d}z = 0,$$
$$\text{for } i,j = 1,2,3,4. \tag{12}$$

Equations (11) can be rewritten in the following matrix form:

$$\begin{Bmatrix} N_{xx} \\ N_{\theta\theta} \\ N_{x\theta} \\ N_{\theta x} \\ M_{xx} \\ M_{\theta\theta} \\ M_{x\theta} \\ M_{\theta x} \end{Bmatrix} - (e_0 a)^2 \nabla^2 \begin{Bmatrix} N_{xx} \\ N_{\theta\theta} \\ N_{x\theta} \\ N_{\theta x} \\ M_{xx} \\ M_{\theta\theta} \\ M_{x\theta} \\ M_{\theta x} \end{Bmatrix} = \left(\begin{bmatrix} A_{11} & A_{12} & A_{13} & A_{14} & B_{11} & B_{12} & B_{13} & B_{14} \\ A_{21} & A_{22} & A_{23} & A_{24} & B_{21} & B_{22} & B_{23} & B_{24} \\ A_{31} & A_{32} & A_{33} & A_{34} & B_{31} & B_{32} & B_{33} & B_{34} \\ A_{41} & A_{42} & A_{43} & A_{44} & B_{41} & B_{42} & B_{43} & B_{44} \\ B_{11} & B_{12} & B_{13} & B_{14} & C_{11} & C_{12} & C_{13} & C_{14} \\ B_{21} & B_{22} & B_{23} & B_{24} & C_{21} & C_{22} & C_{23} & C_{24} \\ B_{31} & B_{32} & B_{33} & B_{34} & C_{31} & C_{32} & C_{33} & C_{34} \\ B_{41} & B_{42} & B_{43} & B_{44} & C_{41} & C_{42} & C_{43} & C_{44} \end{bmatrix} \right.$$

$$+\left(\frac{\alpha_4}{r}\right)\begin{bmatrix} B_{11} & B_{12} & B_{13} & B_{14} & C_{11} & C_{12} & C_{13} & C_{14} \\ 0 & 0 & 0 & 0 & 0 & 0 & 0 & 0 \\ B_{31} & B_{32} & B_{33} & B_{34} & C_{31} & C_{32} & C_{33} & C_{34} \\ 0 & 0 & 0 & 0 & 0 & 0 & 0 & 0 \\ C_{11} & C_{12} & C_{13} & C_{14} & D_{11} & D_{12} & D_{13} & D_{14} \\ 0 & 0 & 0 & 0 & 0 & 0 & 0 & 0 \\ C_{31} & C_{32} & C_{33} & C_{34} & D_{31} & D_{32} & D_{33} & D_{34} \\ 0 & 0 & 0 & 0 & 0 & 0 & 0 & 0 \end{bmatrix}\begin{Bmatrix} \varepsilon^0_{xx} \\ \varepsilon^0_{\theta\theta} \\ \gamma^0_{x\theta} \\ \gamma^0_{x\theta} \\ k_{xx} \\ k_{\theta\theta} \\ k_{x\theta} \\ k_{x\theta} \end{Bmatrix}. \quad (13)$$

The second part of the matrix on the right-hand side of Eq. (13) relates to the inclusion of the $1+z/r$ term instead of $(1z/r)\approx 1$ approximation. It should also be noted that since $N_{x\theta}=N_{\theta x}$ and $M_{x\theta}=M_{\theta x}$ in the Love, Donnell, and Sanders theories, the coefficients $\gamma_{x\theta}$ and $k_{x\theta}$ are multiplied by $1/2$. Considering the values of A_{ij}, B_{ij}, C_{ij}, D_{ij} [Eq. (12)], and Q_{ij} we have

$$\begin{aligned}
&N_{xx}(1-(e_0a)^2\nabla^2)\\
&=C_{\rm R}\varepsilon^0_{xx}+\nu C_{\rm R}\varepsilon^0_{\theta\theta}+(\alpha_4 D_{\rm R}/r)k_{xx}+(\alpha_4\nu D_{\rm R}/r)k_{\theta\theta}, && (14a)\\
&N_{\theta\theta}(1-(e_0a)^2\nabla^2)=\nu C_{\rm R}\varepsilon^0_{xx}+C_{\rm R}\varepsilon^0_{\theta\theta}, && (14b)\\
&N_{x\theta}(1-(e_0a)^2\nabla^2)=G_{\rm R}h\gamma^0_{x\theta}+(\alpha_4 Gh^3/12r)k_{x\theta}, && (14c)\\
&N_{\theta x}(1-(e_0a)^2\nabla^2)=G_{\rm R}h\gamma^0_{x\theta}, && (14d)\\
&M_{xx}(1-(e_0a)^2\nabla^2)\\
&=(\alpha_4 D_{\rm R}/r)\varepsilon^0_{xx}+(\alpha_4\nu D_{\rm R}/r)\varepsilon^0_{\theta\theta}+D_{\rm R}k_{xx}+\nu D_{\rm R}k_{\theta\theta}, && (14e)\\
&M_{\theta\theta}(1-(e_0a)^2\nabla^2)=\nu D_{\rm R}k_{xx}+D_{\rm R}k_{\theta\theta}, && (14f)\\
&M_{x\theta}(1-(e_0a)^2\nabla^2)\\
&=(\alpha_4 G_{\rm R}h^3/12r)\gamma^0_{x\theta}+(G_{\rm R}h^3/12)k_{x\theta}, && (14g)\\
&M_{\theta x}(1-(e_0a)^2\nabla^2)=(G_{\rm R}h^3/12)k_{x\theta}, && (14h)
\end{aligned}$$

where $C_{\rm R}$, $D_{\rm R}$, and $G_{\rm R}$ indicate the shell membrane rigidity, the shell flexural rigidity, and modulus of rigidity (shell modulus), respectively, which are defined as

$$C_{\rm R}=\frac{Eh}{1-\nu^2},\quad D_{\rm R}=\frac{Eh^3}{12(1-\nu^2)},\quad G_{\rm R}=\frac{E}{2(1+\nu)}. \quad (15)$$

Finally, the general nonlocal structural equations can be obtained by substituting the strain components of generalized compatibility equations [ε^0_{ij} and k_{ij} in Eq. (6)] into Eq. (14).

2.4. Hamilton principle

In this subsection, Hamilton's principle is used to obtain the governing equations of the problem. Based on this principle we have

$$\Pi=K, \quad (16)$$

where K is kinetic energy and Π represents the total potential of an elastic system defined as follows:

$$\Pi=U+W, \quad (17)$$

in which U and W are the strain energy function and the potential energy of the external forces (virtual work), respectively. The Lagrangian form of Eq. (16) can be written as

$$\int_{t_1}^{t_2}(\delta U+\delta W-\delta K)\,{\rm d}t=0, \quad (18)$$

where δ is the variation operator and t represents the time. The variations of strain energy, virtual work, and kinetic energy in cylindrical coordinates are expressed as follows:

$$\delta U=\int_{-L}^{L}\int_{0}^{2k\pi}\int_{-h/2}^{h/2}\frac{1}{2}(\sigma_i\delta\varepsilon_i)\,{\rm d}x{\rm d}\theta{\rm d}z, \quad (19a)$$

$$\delta W=-\int_{-L}^{L}\int_{0}^{2k\pi}[p(x,\theta)\delta w]\,{\rm d}x{\rm d}\theta, \quad (19b)$$

$$\delta K=\int_{-L}^{L}\int_{0}^{2k\pi}\int_{-h/2}^{h/2}\rho\,(\dot{u}_j\delta\dot{u}_j)\,{\rm d}x{\rm d}\theta{\rm d}z. \quad (19c)$$

In the following, after the determination of each of these integrals and substituting them in Eq. (18), the final relation of the governing equations will be obtained.

2.4.1. Strain energy

Given the cylindrical coordinates and the insignificance of changes in the direction of the thickness (radial direction), the variables of Eq. (19a) are considered as $i=1,\,2,\,4$ in a symmetric system and are discretized as follows:

$$\delta U=\int_{\Omega}\int_{-h/2}^{h/2}(\sigma_x\delta\varepsilon_x+\sigma_\theta\delta\varepsilon_\theta+\tau_{\theta x}\delta\gamma_{x\theta})\,{\rm d}Z{\rm d}\Omega, \quad (20)$$

where Ω represents the surface area (i.e., ${\rm d}\Omega={\rm d}x{\rm d}\theta$). It should be noted that due to the non-symmetry coordinate system of the Flügge shell theory, the third term on the right side of Eq. (20) is considered as $(\sigma_{x\theta}+\sigma_{\theta x})\delta\varepsilon_{x\theta})$. Therefore, in order to achieve a general relationship that includes all theories, Eq. (20) is rewritten as

$$\begin{aligned}\delta U=&\int_{\Omega}\int_{-h/2}^{h/2}(\sigma_x\delta\varepsilon_x+\sigma_\theta\delta\varepsilon_\theta\\&+(\alpha_4\sigma_{x\theta}+\sigma_{\theta x})\delta\varepsilon_{x\theta})\,{\rm d}Z{\rm d}\Omega. \quad (21)\end{aligned}$$

By inserting the compatibility equations [Eq. (6)] in Eq. (21) and separating them, the strain energy variations are expressed as

$$\begin{aligned}\delta U=&\int_{\Omega}\delta\varepsilon^0_{xx}\int_{-h/2}^{h2}\sigma_x{\rm d}Z{\rm d}\Omega+\int_{\Omega}\delta k_{xx}\int_{-h/2}^{h/2}z\sigma_x{\rm d}Z{\rm d}\Omega\\&+\int_{\Omega}\delta\varepsilon^0_{\theta\theta}\int_{-h/2}^{h/2}\sigma_\theta\,{\rm d}Z{\rm d}\Omega+\int_{\Omega}\delta k_{\theta\theta}\int_{-h/2}^{h/2}z\sigma_\theta\,{\rm d}Z{\rm d}\Omega\end{aligned}$$

$$
\begin{aligned}
&+\int_{\Omega}\alpha_4\delta\varepsilon^0_{x\theta}\int_{-h/2}^{h/2}\sigma_{x\theta}\,\mathrm{d}Z\mathrm{d}\Omega\\
&+\int_{\Omega}\alpha_4\delta k_{x\theta}\int_{-h/2}^{h/2}z\sigma_{x\theta}\,\mathrm{d}Z\mathrm{d}\Omega\\
&+\int_{\Omega}\delta\varepsilon^0_{x\theta}\int_{-h/2}^{h/2}\sigma_{\theta x}\mathrm{d}Z\mathrm{d}\Omega\\
&+\int_{\Omega}\delta k_{x\theta}\int_{-h/2}^{h/2}z\sigma_{x\theta}\,\mathrm{d}Z\mathrm{d}\Omega. \qquad (22)
\end{aligned}
$$

Considering the general definition of resultant stresses and moments in the classical theory of shells, the above relation can be given as

$$
\begin{aligned}
\delta U \;=\; &\int_{\Omega}N_{xx}\delta\varepsilon^0_{xx}\,\mathrm{d}\Omega+\int_{\Omega}N_{\theta\theta}\delta\varepsilon^0_{\theta\theta}\,\mathrm{d}\Omega\\
&+\int_{\Omega}\alpha_4N_{x\theta}\delta\varepsilon^0_{x\theta}\,\mathrm{d}\Omega+\int_{\Omega}N_{\theta x}\delta\varepsilon^0_{x\theta}\,\mathrm{d}\Omega\\
&+\int_{\Omega}M_{xx}\delta k_{xx}\mathrm{d}\Omega+\int_{\Omega}M_{\theta\theta}\delta k_{\theta\theta}\,\mathrm{d}\Omega\\
&+\int_{\Omega}\alpha_4M_{x\theta}\delta k_{x\theta}\,\mathrm{d}\Omega+\int_{\Omega}M_{x\theta}\delta k_{x\theta}\,\mathrm{d}\Omega. \qquad (23)
\end{aligned}
$$

Then, by substituting the strain components of generalized compatibility equations, Eqs. (6) (ε_{ij} and k_{ij}), in Eq. (23) and using the integral by part method, Eq. (23) is discretized.

2.4.2. Virtual work

This part of the potential energy, also known as the work of external forces, is presented in two general types of body forces such as weight, and surface forces (distributed loads) such as hydrostatic pressure applied to the system. These forces can be categorized as

$$
W=W_{\mathrm{b}}+W_{\mathrm{s}}, \qquad (24)
$$

where

$$
\begin{aligned}
W_{\mathrm{b}} \;=\; &\int_{\theta}\left\{\bar{N}_xu+\hat{P}_x\frac{\partial u}{\partial x}+\bar{N}_xv+\hat{P}_x\frac{\partial v}{\partial x}+\bar{N}_xw\right.\\
&\left.+\bar{M}_x\frac{\partial w}{\partial x}+Q_x\frac{\partial^2w}{\partial x^2}\right\}r\,\mathrm{d}\theta\Big|_0^L\\
&+\int_{x}\left\{\bar{N}_\theta u+\hat{P}_\theta\frac{\partial u}{\partial\theta}+\bar{N}_\theta v+\hat{P}_\theta\frac{\partial v}{\partial\theta}+\bar{N}_\theta w\right.\\
&\left.+\bar{M}_\theta\frac{\partial w}{\partial\theta}+Q_\theta\frac{\partial^2w}{\partial\theta^2}\right\}\mathrm{d}x\Big|_0^\theta, \qquad (25a)\\
W_{\mathrm{s}} \;=\; &\int_x\int_\theta(f_xu+f_\theta v+f_zw)r\,\mathrm{d}x\,\mathrm{d}\theta, \qquad (25b)
\end{aligned}
$$

in which $\bar{N}_x$, $\bar{N}_\theta$, $\bar{M}_x$, and $\bar{M}_\theta$ are the forces and bending moments (per unit length) applied over the middle surface; $\hat{P}_x$, $\hat{P}_\theta$, Q_x, and Q_θ are the shear forces applied to the boundaries of the structure; and f_x, f_θ, and f_z determinate the distributed loads.

Herein, regardless of the surface forces and considering the linear buckling analysis with in-plane uniform pre-stress, we can rewrite the virtual work variations carried out by the internal forces as[28]

$$
\delta W_{\mathrm{b}}=\int_{\Omega}(\bar{N}_{xx}\delta\varepsilon_{xnl}+\bar{N}_{\theta\theta}\delta\varepsilon_{\theta nl}+\bar{N}_{x\theta}\delta\gamma_{x\theta nl})\,\mathrm{d}\Omega, \qquad (26)
$$

where ε_{xnl}, $\varepsilon_{\theta nl}$, and $\gamma_{x\theta nl}$ are the nonlinear strains. One can use the nonlinear terms of the main strains defined in the general compatibility relation (Eq. (6)) to introduce them.

Here, due to the reasons like considering just the axial buckling, simplifying the relations, considering the buckling in a cylindrical system under lateral and axial pressures, assuming the conditions where w is constant, $v=0$, and the deformations are also independent of θ. Before the buckling occurs, the following relationships will be established based on Stein's research:[29]

$$
\bar{N}_{xx}=-N^0_{xx},\quad \bar{N}_{\theta\theta}=-N^0_{\theta\theta}=0\rightarrow\delta W=-N^0_{xx}w_{xx}, \qquad (27)
$$

where N_{xx} and $N_{\theta\theta}$ are the axial and transverse critical buckling strain values.

2.4.3. Kinetic energy

The kinetic energy of an object is due to its movement. In Eq. (19c), $\dot{u}_j$ is the velocity of the object in the direction j and the volume integral ρ correspond to its mass. In Newtonian mechanics, macroscopic objects move at a fraction of the speed of light, and kinetic energy is calculated as half of the object's mass in its square of velocity ($K=1/2m\times v^2$). In these cases, in addition to the velocity of the object, a force is applied to it by the fluid or particle passing through the structure, it is necessary to consider the effect of this external force on the body's behavior in order to more accurately solution. In general, the structure and passing fluid are considered as a system. Therefore, in these issues, also known as the problem of fluid-structure interaction (FSI), the velocity and acceleration in the direction of displacement must be the same at the contact point of the structure and fluid, based on the physical principle of consistency condition.[30] Therefore, to achieve the speed of the whole system, we can calculate the velocity of the fluid at the point of contact with the structure.[4] Moreover, both structure and fluid are nanoscopic scales here, and so the effects of size should also be taken into account in the relation. To achieve the equations of motion, the initial definition of kinetic energy is adopted as

$$
K=\frac{1}{2}\rho A\int_0^{2\pi}(\dot{u}_x^2+\dot{u}_\theta^2+\dot{u}_z^2)\,\mathrm{d}z, \qquad (28)
$$

and its variation is

$$
\begin{aligned}
\delta K \;&=\;\frac{1}{2}\rho A\int_0^{2\pi}\delta(\dot{u}_x^2+\dot{u}_\theta^2+\dot{u}_z^2)\,\mathrm{d}z\\
&=\;\frac{1}{2}m\int_0^{2\pi}(2\dot{u}_x\delta\dot{u}_x+2\dot{u}_\theta\delta\dot{u}_\theta+2\dot{u}_z\delta\dot{u}_z)\,\mathrm{d}z
\end{aligned}
$$

$$= m\int_0^{2\pi}(\dot{u}_x\delta\dot{u}_x+\dot{u}_\theta\delta\dot{u}_\theta+\dot{u}_z\delta\dot{u}_z)\,\mathrm{d}z$$
$$\Rightarrow \delta K = m\int_0^{2\pi}(\dot{u}\delta\dot{u}+\dot{v}\delta\dot{v}+\dot{w}\delta\dot{w})\,\mathrm{d}z, \tag{29}$$

where ρ is the density, A is the cross-sectional area, and m represents the mass per unit length. Now, using the material derivation in cylindrical coordinates defined as $\frac{D}{Dt} = \frac{\partial}{\partial t}+\dot{r}\frac{\partial}{\partial r}+\frac{\dot{\theta}}{r}\frac{\partial}{\partial\theta}+\dot{z}\frac{\partial}{\partial z}$, the last relation of Eq. (29) can be discretized.

It should be noted that in order to obtain the equations of motion of a fluid, the momentum equilibrium equation, known as the Navier–Stokes equations, is used in fluid dynamics problems. This equation is expressed in cylindrical coordinates as[31]

$$\begin{aligned}
&\rho\left(\frac{\partial u_r}{\partial t}+u_r\frac{\partial u_r}{\partial r}+\frac{u_\theta}{r}\frac{\partial u_r}{\partial\theta}-\frac{u_\theta^2}{r}+u_z\frac{\partial u_r}{\partial z}\right)\\
&=-\frac{\partial P}{\partial r}+\rho g_r+\mu\left[\frac{1}{r}\frac{\partial}{\partial r}\left(r\frac{\partial u_r}{\partial r}\right)-\frac{u_r}{r^2}\right.\\
&\left.+\frac{1}{r^2}\frac{\partial^2 u_r}{\partial\theta^2}-\frac{2}{r^2}\frac{\partial u_\theta}{\partial\theta}+\frac{\partial^2 u_r}{\partial z^2}\right]\\
&\rho\left(\frac{\partial u_\theta}{\partial t}+u_r\frac{\partial u_\theta}{\partial r}+\frac{u_\theta}{r}\frac{\partial u_\theta}{\partial\theta}-\frac{u_r u_\theta}{r}+u_z\frac{\partial u_\theta}{\partial z}\right)\\
&=-\frac{1}{r}\frac{\partial P}{\partial\theta}+\rho g_\theta+\mu\left[\frac{1}{r}\frac{\partial}{\partial r}\left(r\frac{\partial u_\theta}{\partial r}\right)-\frac{u_\theta}{r^2}\right.\\
&\left.+\frac{1}{r^2}\frac{\partial^2 u_\theta}{\partial\theta^2}-\frac{2}{r^2}\frac{\partial u_r}{\partial\theta}+\frac{\partial^2 u_\theta}{\partial z^2}\right]\\
&\rho\left(\frac{\partial u_z}{\partial t}+u_r\frac{\partial u_z}{\partial r}+\frac{u_\theta}{r}\frac{\partial u_z}{\partial\theta}-\frac{u_r u_\theta}{r}+u_z\frac{\partial u_z}{\partial z}\right)\\
&=-\frac{\partial P}{\partial z}+\rho g_z+\mu\left[\frac{1}{r}\frac{\partial}{\partial r}\left(r\frac{\partial u_z}{\partial r}\right)+\frac{1}{r^2}\frac{\partial^2 u_z}{\partial\theta^2}+\frac{\partial^2 u_z}{\partial z^2}\right].
\end{aligned}\tag{30}$$

According to the studies and experiments,[4,19,32] each of the two sides of the Navier–Stokes equations (Eq. 30), which represent the applied force of fluid obtained by different approaches, can be used in the system's equations of motion.

It can be observed that taking into account the conditions and assumptions in each problem and integrating Eq. (29), the resulting equations will be consistent with the Navier–Stokes equations. Using the material derivative of the components of Eq. (29), the velocities and their variations are given as

$$\begin{aligned}
\dot{u} &= \frac{Du}{Dt}=\frac{\partial u}{\partial t}+\frac{\partial u}{\partial t}\frac{\partial u}{\partial x}+\frac{1}{r}\frac{\partial v}{\partial t}\frac{\partial u}{\partial\theta}+\frac{\partial w}{\partial t}\frac{\partial u}{\partial z},\\
\dot{v} &= \frac{Dv}{Dt}=\frac{\partial v}{\partial t}+\frac{\partial u}{\partial t}\frac{\partial v}{\partial x}+\frac{1}{r}\frac{\partial v}{\partial t}\frac{\partial v}{\partial\theta}+\frac{\partial w}{\partial t}\frac{\partial v}{\partial z},\\
\dot{w} &= \frac{Dw}{Dt}=\frac{\partial w}{\partial t}+\frac{\partial u}{\partial t}\frac{\partial w}{\partial x}+\frac{1}{r}\frac{\partial v}{\partial t}\frac{\partial w}{\partial\theta}+\frac{\partial w}{\partial t}\frac{\partial w}{\partial z},
\end{aligned}\tag{31a}$$

$$\begin{aligned}
\delta\dot{u} &= \frac{D\delta u}{Dt}=\frac{\partial\delta u}{\partial t}+\left(\frac{\partial\delta u}{\partial t}\frac{\partial u}{\partial x}+\frac{\partial u}{\partial t}\frac{\partial\delta u}{\partial x}\right)\\
&+\left(\frac{1}{r}\frac{\partial\delta v}{\partial t}\frac{\partial u}{\partial\theta}+\frac{1}{r}\frac{\partial v}{\partial t}\frac{\partial\delta u}{\partial\theta}\right)\\
&+\left(\frac{\partial\delta w}{\partial t}\frac{\partial u}{\partial z}+\frac{\partial w}{\partial t}\frac{\partial\delta u}{\partial z}\right),\\
\delta\dot{v} &= \frac{D\delta v}{Dt}=\frac{\partial\delta v}{\partial t}+\left(\frac{\partial\delta u}{\partial t}\frac{\partial v}{\partial x}+\frac{\partial u}{\partial t}\frac{\partial\delta v}{\partial x}\right)\\
&+\left(\frac{1}{r}\frac{\partial\delta v}{\partial t}\frac{\partial v}{\partial\theta}+\frac{1}{r}\frac{\partial v}{\partial t}\frac{\partial\delta v}{\partial\theta}\right)\\
&+\left(\frac{\partial\delta w}{\partial t}\frac{\partial v}{\partial z}+\frac{\partial w}{\partial t}\frac{\partial\delta v}{\partial z}\right),\\
\delta\dot{w} &= \frac{D\delta w}{Dt}=\frac{\partial\delta w}{\partial t}+\left(\frac{\partial\delta u}{\partial t}\frac{\partial w}{\partial x}+\frac{\partial u}{\partial t}\frac{\partial\delta w}{\partial x}\right)\\
&+\left(\frac{1}{r}\frac{\partial\delta v}{\partial t}\frac{\partial w}{\partial\theta}+\frac{1}{r}\frac{\partial v}{\partial t}\frac{\partial\delta w}{\partial\theta}\right)\\
&+\left(\frac{\partial\delta w}{\partial t}\frac{\partial w}{\partial z}+\frac{\partial w}{\partial t}\frac{\partial\delta w}{\partial z}\right).
\end{aligned}\tag{31b}$$

By substituting Eqs. (31a) and (31b) into Eq. (29), and after multiplying and separating the parameters, the displacement variations fields caused by the passing fluid are obtained.

Finally, in order to simplify the equations, taking into account the assumptions such as the fact that due to the very thin structure, the variations along the z-direction are negligible and the derivatives relative to z are considered to be zero. In addition, regarding the nano-scale system, the displacement variations of the circumference variable, θ, are also neglected if it is enough small. Then, the relations obtained for the fluid displacement field will be as follows:

$$\begin{aligned}
\delta u:\ & m\left[\frac{\partial^2 u}{\partial t^2}+\frac{\partial^2 u}{\partial t^2}\frac{\partial u}{\partial x}+3\dot{u}\frac{\partial^2 u}{\partial x\partial t}+2\dot{u}\frac{\partial^2 u}{\partial x\partial t}\frac{\partial u}{\partial x}+\dot{u}^2\frac{\partial^2 u}{\partial x^2}\right],\\
\delta v:\ & m\left[\frac{\partial^2 v}{\partial t^2}+\frac{\partial^2 u}{\partial t^2}\frac{\partial v}{\partial x}+2\dot{u}\frac{\partial^2 v}{\partial x\partial t}\right.\\
&\left.+\dot{v}\frac{\partial^2 u}{\partial x\partial t}+2\dot{u}\frac{\partial^2 u}{\partial x\partial t}\frac{\partial v}{\partial x}+\dot{u}^2\frac{\partial^2 v}{\partial x^2}\right],\\
\delta w:\ & m\left[\frac{\partial^2 w}{\partial t^2}+\frac{\partial^2 u}{\partial t^2}\frac{\partial w}{\partial x}+2\dot{u}\frac{\partial^2 w}{\partial x\partial t}\right.\\
&\left.+\dot{w}\frac{\partial^2 u}{\partial x\partial t}+2\dot{u}\frac{\partial^2 u}{\partial x\partial t}\frac{\partial w}{\partial x}+\dot{u}^2\frac{\partial^2 w}{\partial x^2}\right].
\end{aligned}\tag{32}$$

The above relationships can also be obtained by considering the simplified material derivative $\left(\frac{D}{Dt}=\frac{\partial}{\partial t}+\dot{u}\frac{\partial}{\partial x}\right)$, so it can be utilized for different problems such as buckling, vibrations, and bending. In the buckling problem, the time derivatives are eliminated concerning the fact that only the displacement variables are investigated.

It is also worth noting that in this study, for the first time, the effect of the passing fluid on the nanoscale structure has been studied using a cylindrical shell model, and it should be noted that the mass in the final relation of Eq. (29) includes both the structure and fluid. Therefore, these relations with the maintenance of the explained principles will be considered as follows:

$$\delta K = (m_\mathrm{c}+m_\mathrm{f})\int_0^{2\pi}(\dot{u}\delta\dot{u}+\dot{v}\delta\dot{v}+\dot{w}\delta\dot{w})\,\mathrm{d}z, \tag{33}$$

where m_c is the mass of the structure (CNT) and m_f is the mass of the fluid. It is clear that the expression inside the integral

for each mass is related to the velocity of those masses, that is, the mass of the fluid is multiplied by the fluid velocity, and the mass of the structure is multiplied by the velocity of the structure. However, it is noteworthy that for the fluid-structure interaction problems, the velocity at the contact point is intended and calculated, which is equal for both structure and fluid in accordance with molecular physics.

2.4.4. Knudsen number

To investigate the small-scale effects of the nano-fluid flow and for having the slip-boundary condition the velocity correction factor (VCF) should be inserted into the FSI equation of motion multiplied by the flow velocity term. This parameter is introduced as the ratio of the mean flow velocity of fluid passing through the CNT in a slip boundary condition to the mean fluid velocity of the same fluid under a no-slip boundary condition. Thus, the VCF parameter is defined as[32]

$$\begin{aligned}\mathrm{VCF} &= \frac{V_{\mathrm{slip}}}{V_{\mathrm{no-slip}}}\\ &= \frac{1}{Cr(Kn)}\left[4\left(\frac{2-\sigma_v}{\sigma_v}\right)\left(\frac{Kn}{1-bKn}\right)+1\right],\end{aligned} \tag{34}$$

where V_{slip} and $V_{\mathrm{no-slip}}$ are the flow velocities with and without slip boundary conditions, respectively. Also, σ_v and b are the tangential momentum accommodation coefficient and the general slip coefficient, and Cr is the rarefaction coefficient that, by using the Pollard suggestion relation for viscous fluid, is defined as[33]

$$Cr(Kn) = \frac{1}{1+\alpha Kn}, \tag{35}$$

where α is a theoretical constant that is computed as $\alpha = (2/\pi)\,\alpha[\tan^{-1}(\alpha_k Kn^B)]$, in which $\alpha = 64/[3\pi(1-(4/b))]$. In addition, α_k and B are some practical parameters obtained by implementing experimental observations. The Knudsen number and the other unknown parameters in Eqs. (34) and (35) are given in Table 2.

Table 2. The values of nano-flow parameters.[34]

Parameter	Symbol	Range of value
Knudsen number	Kn	0.001–0.01 for liquid 0.001–2 for gas
Tangential momentum accommodation coefficient	σ_v	0.7
general slip coefficient	b	−1
Other parameters	α_k, B	0.4

3. Solution procedure

In the above sections, the field equations were obtained and generalized using the elasticity theories. These equations include a set of differential and algebraic relationships between stresses, strains, and displacements that express specific physics at all points of the object being investigated. Here, first the final equations are presented. Then, the field equations are completed by defining the appropriate boundary conditions, and finally, the non-dimensional form of equations will be analytically solved.

3.1. FSI governing equations

In this subsection, by substituting the results obtained in the previous subsections relating to potential energy (strain energy and virtual work) and kinetic energy into Hamilton principle relation, the final governing equations of the motion and carbon nanotube-passing nanofluid interaction are yielded through the four non-localized theories of Love, Flügge, Donnell, and Sanders. These equations are written after sorting as

$$\begin{aligned}&r^2u_{,xx}+\frac{1-\upsilon}{2}(1+\frac{\alpha_4h^2}{12r^2})u_{,\theta\theta}+\frac{1+\upsilon}{2}rv_{,x\theta}+r\upsilon w_{,x}-\frac{\alpha_4rh^2}{12}w_{,xxx}-\left(\frac{\alpha_4h^2}{24r^2}(1-\upsilon)\right)w_{,x\theta\theta}+\frac{\alpha_2}{4r}\left(N^0_{xx}+N^0_{\theta\theta}\right)\left[\frac{u_{,\theta\theta}}{r}-v_{,x\theta}\right]\\ &=(1-(e_0a)^2\nabla^2)\frac{r^2}{C_{\mathrm{R}}}\left\{m_{\mathrm{f}}(VCF)^2\dot{u}^2\frac{\partial^2u}{\partial x^2}\right\},\end{aligned} \tag{36a}$$

$$\begin{aligned}&\frac{1+\upsilon}{2}ru_{,x\theta}+\left(1+\frac{\alpha_3h^2}{12r^2}\right)v_{,\theta\theta}+\left(1+\frac{\alpha_3\alpha_4h^2}{12r^2}\right)w_{,\theta}+\left[\frac{1-\upsilon}{2}r^2+\frac{h^2}{24}(1-\upsilon)\left[4\alpha_3+3\alpha_4-3\alpha_2\right]\right]v_{,xx}\\ &-\frac{h^2}{12}\left(\alpha_2(\upsilon-1)+\alpha_3(2-\upsilon)+\frac{\alpha_4}{2}(3-\upsilon)\right)w_{,xx\theta}-\frac{\alpha_3h^2}{12r^2}w_{,\theta\theta\theta}\\ &=(1-(e_0a)^2\nabla^2)\frac{r^2}{C_{\mathrm{R}}}\left\{m_{\mathrm{f}}(VCF)^2\dot{u}^2\frac{\partial^2v}{\partial x^2}\right\},\end{aligned} \tag{36b}$$

$$\begin{aligned}&-(1-2\alpha_1)\frac{r^2h^2}{12}\nabla^4w-r\upsilon(\alpha_3-\alpha_4-\alpha_1-\alpha_2)u_{,x}+\left(1+\frac{\alpha_4h^2}{12r^2}\right)v_{,\theta}-\left(1+\frac{\alpha_4h^2}{12r^2}\right)(1-2\alpha_1)w\\ &-\frac{\alpha_4rh^2}{12}u_{,xxx}-\frac{h^2}{12}\left[\alpha_2(\upsilon-1)+\alpha_3(2-\upsilon)+\frac{\alpha_4}{2}(3-\upsilon)\right]v_{,xx\theta}+\frac{\alpha_4\upsilon h^2}{12}w_{,xx}-\frac{\alpha_3h^2}{12r^2}v_{,\theta\theta\theta}\\ &+\frac{\alpha_4h^2}{24r}(1-\upsilon)u_{,x\theta\theta}-\frac{h^2}{12}\left[-3\upsilon+\alpha_4(1-\upsilon)\right]w_{,xx\theta\theta}+\frac{\alpha_6h^2(1-\upsilon)}{12r}u_{,x\theta\theta}-N^0_{xx}w_{,xx}\\ &=(1-(e_0a)^2\nabla^2)\frac{r^2}{C_{\mathrm{R}}}\left\{m_{\mathrm{f}}(VCF)^2\dot{u}^2\frac{\partial^2w}{\partial x^2}\right\}.\end{aligned} \tag{36c}$$

Here, ∇^4 declares the bi-harmonic operator, which is calculated as Laplacian of Laplacian $\nabla^4(\,) = \nabla^2(\nabla^2(\,))$. This expression can be shown as $\nabla^4(\,) = \left(\frac{\partial^2(\,)}{\partial x^2} + \frac{1}{r^2}\frac{\partial^2(\,)}{\partial \theta^2}\right)^2$ in cylindrical coordinates.

3.2. Boundary conditions

The boundary conditions determine the physical occurrence at the boundary of the object. In other words, the applied loads, which physically cause to create the stress, strains, and internal displacement fields, must be considered. Although the formulation of the field equations for each theory is similar, the boundary conditions for each problem will be different. Therefore, determining the appropriate boundary conditions is necessary to solve the problem.

In this study, the essential type of boundary conditions is considered. On the other hand, to analytically solve the equations, the field variables (i.e. u, v, and w) are considered as[35]

$$\begin{aligned} u &= U_{mn}\frac{\partial \Phi(x)}{\partial x}\cos(n\theta),\\ v &= V_{mn}\Phi(x)\sin(n\theta),\\ w &= W_{mn}\Phi(x)\cos(n\theta), \end{aligned} \tag{37}$$

in which U_{mn}, V_{mn}, and W_{mn} are the unknown coefficients that represent the motion altitudes; n is the half circumferential wave; Φ is an axial function, which specifies the geometric boundary conditions. This function is considered as the characteristic function of the structure as follows:[36]

$$\begin{aligned} \Phi \;=\; & a_1\cosh\left(\frac{\lambda_m x}{L}\right) + a_2\cos\left(\frac{\lambda_m x}{L}\right)\\ & - \varsigma_m\left[a_3\sinh\left(\frac{\lambda_m x}{L}\right) + a_4\sin\left(\frac{\lambda_m x}{L}\right)\right], \end{aligned} \tag{38}$$

where a_i ($i = 1, 2, 3, 4$) are constants that are 0, 1, or -1 depending on the structure ends. Moreover, λ_m represents the roots of non-algebraic equations derived from the CNT boundary conditions and ς_m indicates the parameters of the same boundary conditions.

Considering that the purpose of this study is to investigate the effect of external force caused by passing nano-fluid on the mechanical behavior of the nanostructure, to simplify the exact analytical solution, and also with respect to the considered geometry, the simply supported ends (SS) type of boundary conditions is utilized. Hence, Eq. (38) is rewritten as

$$\Phi = \sin\left(\frac{m\pi x}{L}\right). \tag{39}$$

Substituting Eq. (39) in Eq. (37) leads to the values of the following variables:

$$\begin{aligned} u &= U_{mn}\cos\frac{m\pi x}{L}\cos(n\theta),\\ v &= V_{mn}\sin\frac{m\pi x}{L}\sin(n\theta),\\ w &= W_{mn}\sin\frac{m\pi x}{L}\cos(n\theta). \end{aligned} \tag{40}$$

3.3. Solution of the dimensionless governing equations

Having developed the theories, we are in a position to solve Eqs. (36a)–(36c) with boundary conditions of simply supported ends adopting the analytical approach [Eq. (40)]. Before proceeding, it is convenient first to define the following dimensionless quantities:

$$\begin{aligned} & x^* = \frac{x}{L},\quad \theta^* = \frac{\theta}{r},\quad \{u,v,w\}^* = \frac{\{u,v,w\}}{h},\\ & \beta_1 = \frac{h}{r},\quad \beta_2 = \frac{L}{r},\quad \beta_3 = \frac{h}{L},\\ & \beta_4 = \frac{h}{(r)^2},\quad \beta_5 = \frac{L}{(r)^2},\quad \beta_6 = \frac{h}{(L)^2},\\ & e_n = \frac{e_0 a}{L},\quad \dot{u}_{\mathrm{f}}^* = \sqrt{\frac{m_{\mathrm{f}}}{C_{\mathrm{R}}}}\dot{u}_{\mathrm{f}},\\ & \nabla^{*2} = \left(\frac{\partial^2}{\partial x^{*2}} + \beta_5^2\frac{\partial^2}{\partial \theta^{*2}}\right),\\ & \nabla^{*4} = \nabla^{*2}\cdot\nabla^{*2} = \left(\frac{\partial^4}{\partial x^{*4}} + 2\beta_5^2\frac{\partial^4}{\partial x^{*2}\partial \theta^{*2}} + \beta_5^4\frac{\partial^4}{\partial \theta^{*4}}\right). \end{aligned} \tag{41}$$

Moreover, using the above non-dimensional parameters, the boundary conditions in dimensionless form make displacement variables [Eq. (40)] as

$$\begin{aligned} u^* &= U_{mn}\cos(m\pi x^*)\cos(nr\theta^*),\\ v^* &= V_{mn}\sin(m\pi x^*)\sin(nr\theta^*),\\ w^* &= W_{mn}\sin(m\pi x^*)\cos(nr\theta^*). \end{aligned} \tag{42}$$

Considering non-dimensional parameters of Eq. (41) and substituting Eq. (42) into Eqs. (36a)–(36c), the final dimensionless governing equations are reached as

$$\begin{aligned} & \cos(m\pi x^*)\cos(nr\theta^*)\left\{-(m\pi)^2 U_{mn} - \frac{1-\upsilon}{2}\beta_5^2\left(1+\frac{\alpha_4}{12}\beta_1^2\right)(nr)^2 U_{mn} + \frac{1+\upsilon}{2}\beta_5(m\pi)(nr)V_{mn}\right.\\ & \left. + \upsilon\beta_2(m\pi)W_{mn} + \frac{\alpha_4}{12}\beta_1\beta_3(m\pi)^3 W_{mn} + \frac{\alpha_4}{24}(1-\upsilon)\beta_4^2\beta_5(m\pi)(nr)^2 W_{mn}\right.\\ = \; & \left.\left[1 - e_n^2\left((m\pi)^2 + \beta_5^2(nr)^2\right)\right]\left[-(VCF)^2\dot{u}_{\mathrm{f}}^{*2}(m\pi)^2 U_{mn}\right]\right\}, \end{aligned} \tag{43a}$$

$$\sin(m\pi x^*)\sin(nr\theta^*)\left\{\frac{1+\upsilon}{2}\beta_5((m\pi)(nr)U_{mn}) - \beta_5^2(1+\frac{\alpha_4}{12}\beta_1^2)((nr)^2 V_{mn})\right.$$

$$
\begin{aligned}
&-\beta_2\beta_5\left(1+\frac{\alpha_3\alpha_4}{12}\beta_1^2\right)((nr)W_{mn})-\frac{1-\upsilon}{2}\left[1+\frac{\beta_1^2}{12}(4\alpha_3+3\alpha_4-3\alpha_2)\right]((m\pi)^2V_{mn})\\
&-\frac{\beta_1\beta_3\beta_5}{12}\left(\alpha_2(\upsilon-1)+\alpha_3(2-\upsilon)+\frac{\alpha_4}{2}(\upsilon-3)\right)((m\pi)^2(nr)W_{mn})-\frac{\alpha_3}{12}\beta_1\beta_4\beta_5^2((nr)^3W_{mn})\\
=&\ \left[1-e_n^2\left((m\pi)^2+\beta_5^2(nr)^2\right)\right]\left[-(VCF)^2\dot{u}_{\mathrm{f}}^{*2}((m\pi)^2V_{mn})\right]\Bigg\}, \qquad (43b)\\
&\sin(m\pi x^*)\cos(nr\theta^*)\Bigg\{-\frac{(1-2\alpha_1)}{12}\beta_3^2\left(((m\pi)^4W_{mn})+2\beta_5^2((m\pi)^2(nr)^2W_{mn})+\beta_5^4((nr)^4W_{mn})\right)\\
&+\beta_2\upsilon(\alpha_3-\alpha_4-\alpha_1-\alpha_2)((m\pi)U_{mn})+\beta_2\beta_5((nr)V_{mn})-(1-2\alpha_1)\beta_2^2\left(1+\frac{\alpha_4}{12}\beta_1^2\right)W_{mn}\\
&-\frac{\alpha_4}{12}\beta_1\beta_3((m\pi)^3U_{mn})+\frac{\beta_1\beta_4}{12}\left[\alpha_2(\upsilon-1)+\alpha_3(2-\upsilon)+\frac{\alpha_4}{2}(\upsilon-3)\right]((m\pi)^2(nr)V_{mn})\\
&+\frac{2\alpha_4}{12}\beta_1^2\beta_5^2((nr)^2W_{mn})+\frac{\alpha_3}{12}\beta_1\beta_4\beta_5^2((nr)^3V_{mn})+\frac{\beta_2\beta_4^2}{12}(1-\upsilon)((m\pi)(nr)^2U_{mn})\alpha_6\left[1-\frac{\alpha_4}{2}\right]\\
&-\frac{\beta_4^2}{12}\left[-3\upsilon+\alpha_4(1-\upsilon)\right]((m\pi)^2(nr)^2W_{mn})\\
=&\ \left[1-e_n^2\left((m\pi)^2+\beta_5^2(nr)^2\right)\right]\left[-(VCF)^2\dot{u}_{\mathrm{f}}^{*2}((m\pi)^2W_{mn})-N_{xx}^0((m\pi)^2W_{mn})\right]\Bigg\}. \qquad (43c)
\end{aligned}
$$

To achieve the solution of the above equations, the following relations are rendered and solved by forming the coefficient matrix and factorizing the trigonometric expression:

$$
\begin{bmatrix}\cos\frac{m\pi x}{L}\cos(n\theta)\\ \sin\frac{m\pi x}{L}\sin(n\theta)\\ \sin\frac{m\pi x}{L}\cos(n\theta)\end{bmatrix}\begin{bmatrix}F_{11}&F_{12}&F_{13}\\F_{21}&F_{22}&F_{23}\\F_{31}&F_{32}&F_{33}\end{bmatrix}\begin{bmatrix}U_{mn}\\V_{mn}\\W_{mn}\end{bmatrix}=\begin{bmatrix}0\\0\\0\end{bmatrix}, \qquad (44)
$$

where

$$
\begin{aligned}
F_{11}=&-(m\pi)^2-\frac{1-\upsilon}{2}\beta_5^2\left(1+\frac{\alpha_4}{12}\beta_1^2\right)(nr)^2-\left[1-e_n^2\left((m\pi)^2+\beta_5^2(nr)^2\right)\right]\left[-(VCF)^2\dot{u}_{\mathrm{f}}^{*2}(m\pi)^2\right],\quad F_{12}=+\frac{1+\upsilon}{2}\beta_5(m\pi)(nr),\\
F_{13}=&+\upsilon\beta_2(m\pi)+\frac{\alpha_4}{12}\beta_1\beta_3(m\pi)^3+\frac{\alpha_4}{24}(1-\upsilon)\beta_4^2\beta_5(m\pi)(nr)^2,\quad F_{21}=\frac{1+\upsilon}{2}\beta_5((m\pi)(nr)),\\
F_{22}=&-\beta_5^2\left(1+\frac{\alpha_3}{12}\beta_1^2\right)((nr)^2)-\frac{1-\upsilon}{2}\left[1+\frac{\beta_1^2}{12}(4\alpha_3+3\alpha_4-3\alpha_2)\right]((m\pi)^2)\\
&-\left[1-e_n^2\left((m\pi)^2+\beta_5^2(nr)^2\right)\right]\left[-(VCF)^2\dot{u}_{\mathrm{f}}^{*2}((m\pi)^2)-N_{\theta\theta}^0\beta_2^2\right],\\
F_{23}=&-\beta_2\beta_5\left(1+\frac{\alpha_3\alpha_4}{12}\beta_1^2\right)((nr))-\frac{\beta_1\beta_3\beta_5}{12}\left(\alpha_2(\upsilon-1)+\alpha_3(2-\upsilon)-\frac{\alpha_4}{2}(3-\upsilon)\right)((m\pi)^2(nr))\\
&-\frac{\alpha_3}{12}\beta_1\beta_4\beta_5^2((nr)^3)-\left[1-e_n^2\left((m\pi)^2+\beta_5^2(nr)^2\right)\right]\left[-N_{\theta\theta}^0(\beta_2\beta_5(nr))\right],\\
F_{31}=&+\beta_2\upsilon(\alpha_3-\alpha_4-\alpha_1-\alpha_2)(m\pi)-\frac{\alpha_4}{12}\beta_1\beta_3((m\pi)^3)+\frac{\beta_2\beta_4^2}{12}(1-\upsilon)((m\pi)(nr)^2)\alpha_6\left[1-\frac{\alpha_4}{2}\right],\\
F_{32}=&+\beta_2\beta_5((nr))+\frac{\beta_1\beta_4}{12}\left[\alpha_2(\upsilon-1)+\alpha_3(2-\upsilon)+\frac{\alpha_4}{2}(3-\upsilon)\right]((m\pi)^2(nr))+\frac{\alpha_3}{12}\beta_1\beta_4\beta_5^2((nr)^3),\\
F_{33}=&-\frac{(1-2\alpha_1)}{12}\beta_3^2\left(((m\pi)^4)+2\beta_5^2((m\pi)^2(nr)^2)+\beta_5^4((nr)^4)\right)-(1-2\alpha_1)\beta_2^2\left(1+\frac{\alpha_4}{12}\beta_1^2\right)\\
&-\frac{2\alpha_4}{12}\beta_1^2\beta_5^2((nr)^2)-\frac{\beta_4^2}{12}\left[-3\upsilon+\alpha_4(1-\upsilon)\right]((m\pi)^2(nr)^2)\\
&-\left[1-e_n^2\left((m\pi)^2+\beta_5^2(nr)^2\right)\right]\left[-(VCF)^2\dot{u}_{\mathrm{f}}^{*2}((m\pi)^2)-N_{xx}^0((m\pi)^2)\right]. \qquad (45)
\end{aligned}
$$

4. Numerical results and discussion

In this section, the axial buckling behavior of the carbon nanotube conveying nanofluid is discussed. For this purpose, all the parameters are used in dimensionless form. By utilizing the equation of motion of CNT, the effects of nonlocal dimensionless parameters, e_n and Kn, the effect of nanofluid velocity, the effects of circumferential and longitudinal half wave numbers, the CNT aspect ratio, and also bending rigidity effects on

the critical buckling strain are studied. To analyze the effect of existence, scale size, and velocity of the flowing fluid on the critical buckling loads and mode shapes of CNT buckling, the flowing fluid is assumed to be water. Moreover, water and acetone as liquid flow and air as gas flow are considered to study the fluid density.

The material and geometric parameters of carbon nanotube and fluid are given in Table 3.

Table 3. Material and geometrical properties of carbon nanotube and the flowing fluid.

Parameter	Symbol	Value	Unit
CNT Young's modulus	E	5.5	TPa
CNT diameter	d	6.78	Å
CNT thickness	h	0.66	Å
Poisson's ratio	υ	0.19	–
CNT mass density	ρ_{c}	2.3	g·cm^{-3}
Water mass density	ρ_{w}	1	g·cm^{-3}
Acetone mass density	ρ_{ace}	0.79	g·cm^{-3}
Air mass density	ρ_{air}	0.001169	g·cm^{-3}

4.1. Validation of present results

In this subsection, our obtained numerical results of critical buckling strains are compared with those of molecular dynamic (MD) simulation results.[20] To this end, the passing nanofluid is ignored and then the obtained results of MD simulations and nonlocal shell theories of Love, Flügge, Donnell, and Sanders are shown in Table 4.

According to observations of Silvestre *et al.*,[20] the use of Donnell's theory leads to accurate results only for modes of the high circumferential half-wave number n. In addition, Pellicano and Amabili[37] revealed that the condition $n^2 \gg 1$ must be satisfied in order to have fairly good accuracy and proposed that $n \geq 1$ is adequate. Herein, to compare the results of the four-mentioned theories with the results from MD simulation, the values of the circumferential half-wave number n and the longitudinal half-wave number m are considered to equal 10 and 1, respectively. From Table 4, it can be seen that the critical buckling strains are in good agreement with the MD simulation results. To achieve the best result in terms of the agreement with the results of the molecular dynamics, different values of the internal characteristic length parameter (e_0a) of the nanotubes were investigated and the closest answers to the molecular simulation results are shown in Table 4. Moreover, the results show that the proposed Eqs. (36a)–(36c) could capture correctly the length-dependent buckling strains of CNTs for the mode of shell-type buckling. It can also be found that the available models are unable to indicate the correct trend in critical axial buckling strains of carbon nanotubes with a specific length if the correct value of the parameter of e_0a is not considered.

Table 4. Comparison between critical buckling strain of CNT (5,5) obtained from MD simulations and proposed nonlocal Love, Flügge, Donnell, and Sanders shell cylindrical theories ($m = 1$, $n = 10$).

Length (Å)	MD	Proposed Eq. (43)											
		Love shell theory			Flügge shell theory			Donnell shell theory			Sanders shell theory		
		e_0a (nm)	LST	$\frac{\text{LST}}{\text{MD}}$	e_0a (nm)	FST	$\frac{\text{FST}}{\text{MD}}$	e_0a (nm)	DST	$\frac{\text{DST}}{\text{MD}}$	e_0a (nm)	SST	$\frac{\text{SST}}{\text{MD}}$
16.09	0.08146	0.7	0.08957	1.09	1.0	0.08259	1.014	1.0	0.08331	1.02	1.0	0.08140	0.999
21.04	0.07528	1.0	0.07462	0.99	1.4	0.07188	0.95	1.4	0.07251	0.96	1.4	0.07084	0.94
28.46	0.06992	1.4	0.06946	0.99	1.9	0.07130	1.019	1.9	0.07193	1.03	1.9	0.07027	1.005
40.83	0.06507	2.1	0.06343	0.975	2.8	0.06751	1.037	2.9	0.06349	0.98	2.8	0.06654	1.02
53.21	0.05499	3.0	0.05275	0.96	4.1	0.05346	0.97	4.1	0.05392	0.98	4.0	0.05535	1.006
77.96	0.04208	4.9	0.04243	1.008	6.9	0.04170	0.99	6.8	0.04207	0.999	6.8	0.04234	1.006
102.71	0.02494	8.5	0.02447	0.98	11.7	0.02487	0.997	11.8	0.02466	0.989	11.6	0.02494	1.0
115.09	0.01929	10.7	0.01938	1.004	14.9	0.01918	0.994	14.9	0.01935	1.003	14.8	0.01917	0.993
176.97	0.00821	25.4	0.008199	0.999	34.9	0.00820	0.998	35	0.00823	1.002	34.6	0.00823	1.002
238.82	0.00470	45.2	0.004698	0.999	62.1	0.00471	1.002	62.4	0.00470	1.0	61.6	0.00470	1.0
362.54	0.00250	94	0.002497	0.998	129.2	0.00250	1.0	134.8	0.00250	1.0	133.3	0.00250	1.0

4.2. The effect of half-wave numbers

In this subsection, in order to investigate the amount of efficiency of the longitudinal (m) and circumferential (n) half-wave numbers on the critical buckling load, the variation amount of it is considered at the 20 first buckling modes of CNT. For this purpose, first the m value is considered to equal 1, and n is increased from 1 to 20. It is observed that up to $n = 5$ for the Love shell theory, and $n = 2$ for the rest mentioned theories the value of critical buckling decreases and then the upward trend takes place. If the circumferential half-wave number is put to equal 1 and the longitudinal half-wave changes from 1 to 20, the critical buckling load will always have a decreasing trend. The yielded results are listed in Tables 5 and 6, respectively. It should be noted that these results are obtained for a CNT (5,5) with a length of 16.09 nm.

Table 5. Comparison between critical buckling strain of CNT (5,5) obtained from Love, Flügge, Donnell, and Sanders theories for various circumferential half-wave number n.

n	Critical buckling load			
	LST	FST	DST	SST
1	0.3958	0.0114	0.0115	0.01143
2	0.1282	0.0027	0.0043	0.0028
3	0.0663	0.0071	0.0080	0.0064
4	0.0477	0.0130	0.0137	0.0121
5	0.0437	0.0205	0.0212	0.0195
6	0.0465	0.0296	0.0303	0.0286
7	0.0535	0.0404	0.0411	0.0393
8	0.0635	0.0528	0.0535	0.0517
9	0.0759	0.0669	0.0676	0.0657
10	0.0905	0.0826	0.0833	0.0814
11	0.1070	0.1000	0.1007	0.0987
12	0.1254	0.1190	0.1198	0.1177
13	0.1457	0.1397	0.1405	0.1384
14	0.1677	0.1621	0.1629	0.1607
15	0.1915	0.1861	0.1869	0.1846
16	0.2169	0.2118	0.2126	0.2102
17	0.2441	0.2391	0.2399	0.2375
18	0.2730	0.2681	0.2689	0.2664
19	0.3036	0.2987	0.2996	0.2970
20	0.3359	0.3310	0.3319	0.3292

Table 6. Comparison between critical buckling strain of CNT (5,5) obtained from Love, Flügge, Donnell, and Sanders theories for various longitudinal half-wave number (m).

m	Critical buckling load			
	LST	FST	DST	SST
1	0.3958	0.0114	0.0115	0.01143
2	0.0424	0.0096	0.0103	0.0101
3	0.0090	0.0041	0.0042	0.0041
4	0.0031	0.0020	0.0020	0.0019
5	0.0014	0.0011	0.0011	0.0011
6	0.0009	0.0008	0.0008	0.0008
7	0.0006	0.0006	0.0006	0.0006
8	0.0005	0.0005	0.0005	0.0005
9	0.0005	0.0005	0.0005	0.0005
10	0.0004	0.0004	0.0004	0.0004
11	0.0004	0.0004	0.0004	0.0004
12	0.0004	0.0004	0.0004	0.0004
13	0.0004	0.0004	0.0004	0.0004
14	0.0004	0.0004	0.0004	0.0004
15	0.0004	0.0004	0.0004	0.0004
16	0.0004	0.0004	0.0004	0.0004
17	0.0004	0.0004	0.0004	0.0004
18	0.0004	0.0004	0.0004	0.0004
19	0.0004	0.0004	0.0004	0.0004
20	0.0004	0.0004	0.0004	0.0004

For a better visibility, these results are shown in Figs. 2 and 3. In these figures, the dimensionless critical buckling strain variations with increasing the circumferential and longitudinal half-wave numbers are illustrated. As can be seen in Fig. 2, e.g., for the Sanders theory, the critical buckling load values at $n = 1$ and $n = 2$ are 0.01143 and 0.002827, respectively, and at $n = 3$ its value increases to 0.006358. This process will then consistently increase by enhancing the n value. This is also the matter in other theories, with the difference that the increasing trend of the critical buckling strain starts from $n = 5$ in Love theory. In Fig. 3, it can be identified that by increasing the amount of longitudinal half-wave number, the critical buckling strain value is always reduced. The reduction rate decreases after $m = 2$ and the critical buckling values are almost the same for all the theories from $m = 10$ onwards.

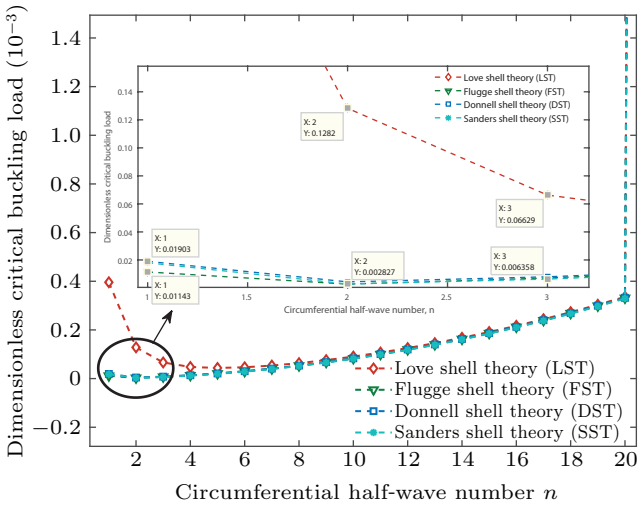


Fig. 2. Dimensionless critical buckling strain of shell cylindrical CNT against the circumferential half-wave number n considering nonlocal Love, Flügge, Donnell, and Sanders shell theories.

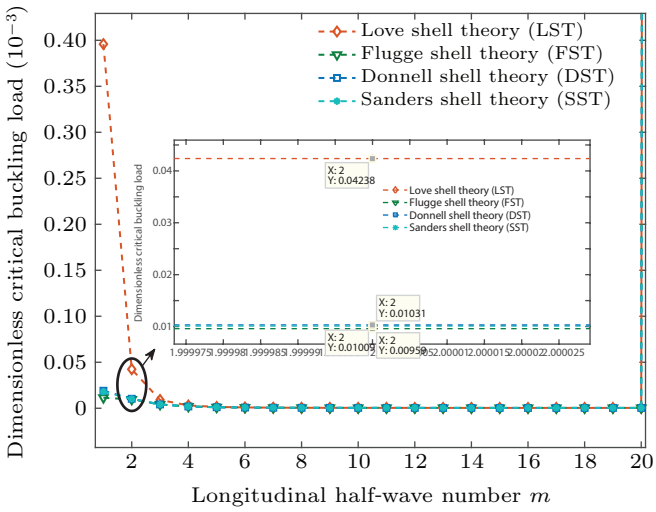


Fig. 3. Dimensionless critical buckling strain of shell cylindrical CNT against the longitudinal half-wave number m considering nonlocal Love, Flügge, Donnell, and Sanders shell theories.

In Fig. 4, changes in dimensionless critical buckling strain value are shown relative to the simultaneous increase of the longitudinal and circumferential half-wave numbers. With this simultaneous increase, the buckling mode shape of shell cylindrical carbon nanotubes can be observed in modes 1 up to 10 considering all the four theories. As shown in this figure, by increasing the mode shape number, the critical value of the buckling load is reduced, so that the process gradually progresses to the smoothing state. It is noticeable that the highest critical buckling load is related to the first mode shape ($m = n = 1$). These maximum values are 0.09047, 0.08331, 0.08259, and 0.0814 for the nonlocal theories of Love, Donnell, Flügge, and Sanders, respectively.

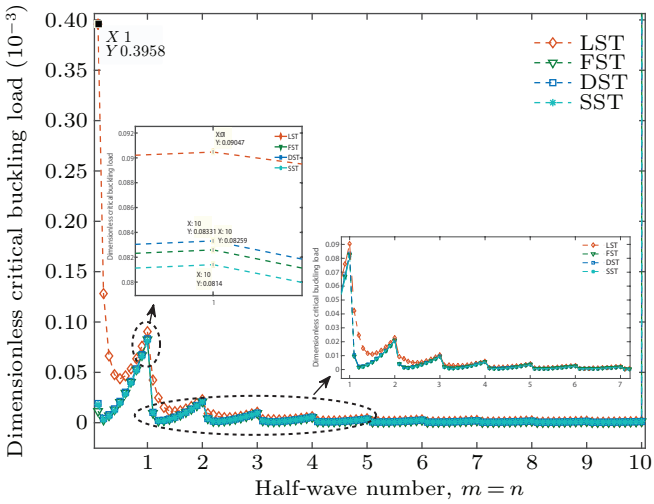


Fig. 4. Dimensionless critical buckling strain of shell cylindrical CNT against the same half-wave numbers ($m = n$) considering nonlocal Love, Flügge, Donnell, and Sanders shell theories.

The maximum critical buckling strain values of modes 1 to 10 are listed in Table 7 for each mentioned nonlocal shell theory.

Table 7. The maximum value of dimensionless critical buckling strain values in mode shapes 1 to 10 for nonlocal shell theories of Love (LST), Flügge (FST), Donnell (DST), and Sanders (SST).

Mode	Maximum of the critical buckling strain			
($m = n$)	LST	FST	DST	SST
1	0.09047	0.08259	0.08331	0.08140
2	0.02288	0.02092	0.02110	0.02062
3	0.01037	0.009501	0.00958	0.009366
4	0.005988	0.005504	0.005548	0.005427
5	0.00396	0.003654	0.003682	0.003604
6	0.002858	0.00265	0.002668	0.002614
7	0.002194	0.002044	0.002057	0.002017
8	0.001762	0.001652	0.001661	0.00163
9	0.001467	0.001382	0.001389	0.001365
10	0.001255	0.00119	0.001194	0.001175

4.3. The effect of passing fluid

As mentioned above, in this study, the effect of flowing nanofluid on the buckling of the shell cylindrical carbon nanotube is investigated, for the first time. Therefore, first this subsection examines that the system critical buckling occurs at how much fluid flow velocity is and how the increasing fluid speed affects the system buckling. For this purpose, the nanoscale characteristic parameters for the structure (e_n) and the fluid (Kn) are considered to equal 1 and 0.05, respectively.

The obtained results of the first five buckling modes for the CNT lengths of 16.09, 21.04, and 28.46 Å are presented in Table 8 based on the four nonlocal theories of Love, Flügge, Donnell, and Sanders. These results show the velocity value of the flowing fluid in which the system buckling has happened. It can be observed that the fluid velocity value in which the critical buckling strain has taken place is decreased by increasing the buckling mode number. In addition, it is found that the critical buckling load occurs in a more fluid speed value for the longer carbon nanotubes. It means that more fluid velocity is needed to reach the critical buckling load if the longer carbon nanotube is selected. Moreover, the highest fluid flow velocity is related to the considered nonlocal shell cylindrical theories of Love, Flügge, Donnell, and Sanders, respectively. On the other hand, Fig. 5 illustrates that under a given condition such as the specified structure length, the nonlocal parameter, and the Knudsen number, the increase in the velocity of the fluid passing through the carbon nanotube increases the critical load of buckling. In Fig. 5, it can be observed that approximately up to the non-dimensional velocity of the nanofluid of 0.01, the value of the critical buckling strain is almost constant, and then it is increased by increasing the nanofluid flow velocity.

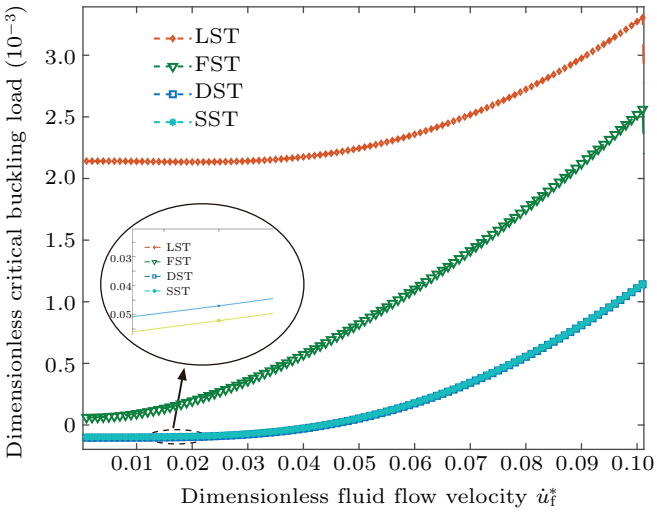


Fig. 5. Dimensionless critical buckling strain of shell cylindrical CNT against dimensionless nanofluid flow velocity considering nonlocal Love, Flügge, Donnell, and Sanders shell theories.

Table 8. Dimensionless fluid velocity for the first five buckling modes of CNT (5,5) using various CNT lengths and various nonlocal shell cylindrical theories considering $e_n = 1$ and $Kn = 0.05$.

Mode	Dimensionless fluid velocity											
	Love shell theory			Flügge shell theory			Donnell shell theory			Sanders shell theory		
($m = n$)	Length (Å)			Length (Å)			Length (Å)			Length (Å)		
	16.09	21.04	28.46	16.09	21.04	28.46	16.09	21.04	28.46	16.09	21.04	28.46
1	0.1605	0.2607	0.4429	0.0154	0.2471	0.4196	0.0638	0.0956	0.1387	0.0620	0.0912	0.1270
2	0.0595	0.0928	0.1413	0.0014	0.0024	0.0018	0.0029	0.0037	0.0050	0.0025	0.0028	0.0035
3	0.0281	0.0468	0.0831	0.0011	0.0016	0.0024	0.0016	0.0022	0.0035	0.0014	0.0019	0.0029
4	0.0033	0.0057	0.0105	0.0011	0.0016	0.0026	0.0013	0.0020	0.0032	0.0012	0.0018	0.0029
5	0.0021	0.0034	0.0061	0.0011	0.0016	0.0027	0.0013	0.0019	0.0031	0.0012	0.0018	0.0029

4.4. Nano-scale effects of structure and fluid

In this subsection, the effects of scale-size effects on the critical buckling load of the system are investigated. In this regard, the scale of the structure and the fluid are studied separately and simultaneously. In order to investigate the nano-scale in structure and fluid, variations of the nonlocal parameter e_0a and Knudsen numbers Kn are considered.

4.4.1. Effect of nonlocal parameter

As mentioned above, to make the model more realistic, the nonlocal parameter e_0a needs to be calibrated such that the nonlocal shell model predicts the results of MD simulations. Here, using MATLAB programming the most proper value for the nonlocal parameter is determined. From the values in Table 4, the developed nonlocal shell model is capable of predicting the results of MD simulations provided that the nonlocal parameter is properly calibrated. It indicates that the axially critical buckling strains of CNTs significantly depend on the small-size effects of the structure, especially when its aspect ratio decreases. It means the bigger values of the nonlocal parameter should be considered for the longer CNTs with the same radius. Moreover, Hu *et al*. studied the flexural wave propagation in armchair (5,5) and (10,10) SWCNTs for a wide range of wave numbers by using the nonlocal beam models and the MD simulations.[38] They proposed the scale coefficient $e = 0.288$ for a wide range of wavelengths from ~ 0.2 nm to ~ 70 nm. Since e_0 is dependent on the material of the structure, this parameter can be considered as a constant parameter for carbon nanotubes. Hence, the change of the e_0a is due to variation of a, which indicates the internal length (such as the web parameter and crystalline distance). Therefore, it is inferred and justified that the value of parameter a is increased by enhancing the carbon nanotube length.

On the other hand, when the length of the nanotube is constant, the change of the nonlocal parameter can affect the critical buckling strain value. In Fig. 6, the CNT length is considered to equal 16.09 (Å) and it can be seen that the critical axially buckling load is decreased by increasing the nonlocal parameter (e_0a). As shown in Fig. 6, a larger critical buckling load is obtained respectively using LST, DST, FST, and SST theories and according to the obtained results in Table 4, it can be revealed that the accuracy of the results is reduced, simultaneously. It means that the order of the theories' accuracy is Sanders, Flügge, Donnell, and Love. For example, for an SWCNT (5,5) shown in Fig. 6, the dimensionless critical buckling strain value is 0.02114, 0.02145, 0.02164, and 0.0235 respectively for SST, FST, DST, and LST at nonlocal parameter value of 10. It should be noted that the results are obtained by inserting VCF = 1. From Eq. (34), the parameter of the velocity correction factor (VCF) will be equal to 1 if the parameter of the Knudsen number is considered to be zero.

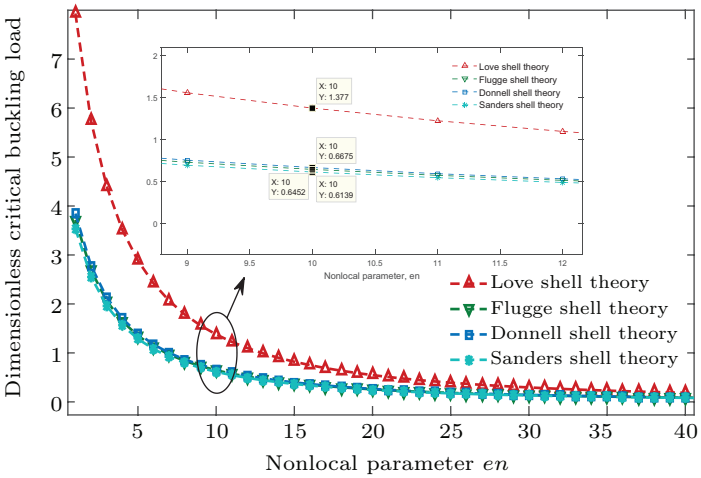


Fig. 6. Dimensionless critical buckling strain of shell cylindrical CNT against nonlocal parameter, e_0a, considering nonlocal Love, Flügge, Donnell, and Sanders theories.

4.4.2. Effect of Knudsen number

In this subsection, we investigate the size effect of nano-flow with a nonzero Kn on the dynamic response of a nanotube conveying a liquid, herein water. Figure 7 illustrates that the non-dimensional critical buckling load of the system increases as the value of the Knudsen number increases. This means that, firstly, taking into account the small scale of the flowing fluid, a greater amount of critical buckling load is yielded. From this figure, it can be detected that considering the slip velocity could lead to appreciable effects on the general dynamic response of the CNT conveying nano-flow. It means that the considered coupled fluid-structure interaction model predicts that CNT conveying nano-flow would lose its stability later than that predicted by continuum plug flow theory or without considering the flowing fluid through CNT. This means that the system loses its stability later and reaches the critical buckling strain value later.

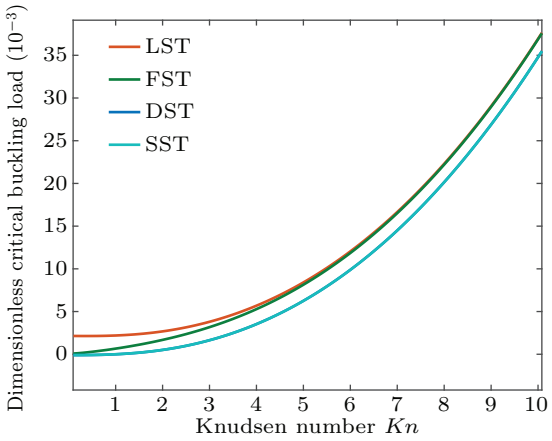


Fig. 7. Dimensionless critical buckling strain of shell cylindrical CNT against Knudsen number, Kn, considering nonlocal Love, Flügge, Donnell, and Sanders theories.

Moreover, it is noticeable that after about $Kn = 6$ the critical value of the buckling obtained from the Love, Flügge, and

Donnell shell theories will be equal to each other, approximately. For the Sanders shell theory, in which two rotations of β_x and β_z are considered, the critical buckling load values will be less.

4.4.3. Simultaneous effects of nonlocal parameter and Knudsen number

In this subsection, we would analyze the small-scale effects on both elastic structure and fluid dynamic responses of CNT conveying liquid nano-flow. Figure 8 shows the dimensionless critical buckling strain of a CNT conveying fluid, herein, water against dimensionless mean flow velocity for nonlocal shell theories of Love, Flügge, Donnell, and Sanders. To better compare the simultaneous effects of the dimensionless parameters of the Eringen nonlocal parameter and Knudsen number, the values of them are considered as (a) $e_n = 0$ and $Kn = 0$, (b) $e_n = 0.5$ and $Kn = 0$, (c) $e_n = 0$ and $Kn = 0.01$, and (d) $e_n = 0.5$ and $Kn = 0.01$.

As it was expected from the results obtained in Subsection 4.3, Fig. 8(a) illustrates that by increasing fluid velocity the carbon nanotube-containing nanofluid would reach a critical amount of buckling load, later, and thus the system would be more stable. In Fig. 8(b), it is seen that with considering $e_n = 0.5$ and $Kn = 0$, the non-dimensional system critical buckling load is decreased by increasing dimensionless flowing fluid speed. With a comparison between Figs. 8(a) and 8(b) it is obvious that by enhancing the nonlocal parameter as an example, for $\dot{u}_f^* = 0$ the dimensionless critical buckling strain is closed to origin using all mentioned shell theories, and for $\dot{u}_f^* = 10$ those values are reduced about to -0.98 utilizing Love, Flügge, Donnell, and Sanders shell theories. Thus, it can be deduced that increasing the amount of the nonlocal parameter meanwhile increasing the velocity of the flowing fluid inside the structure will have a greater effect on the critical values of the buckling strains.

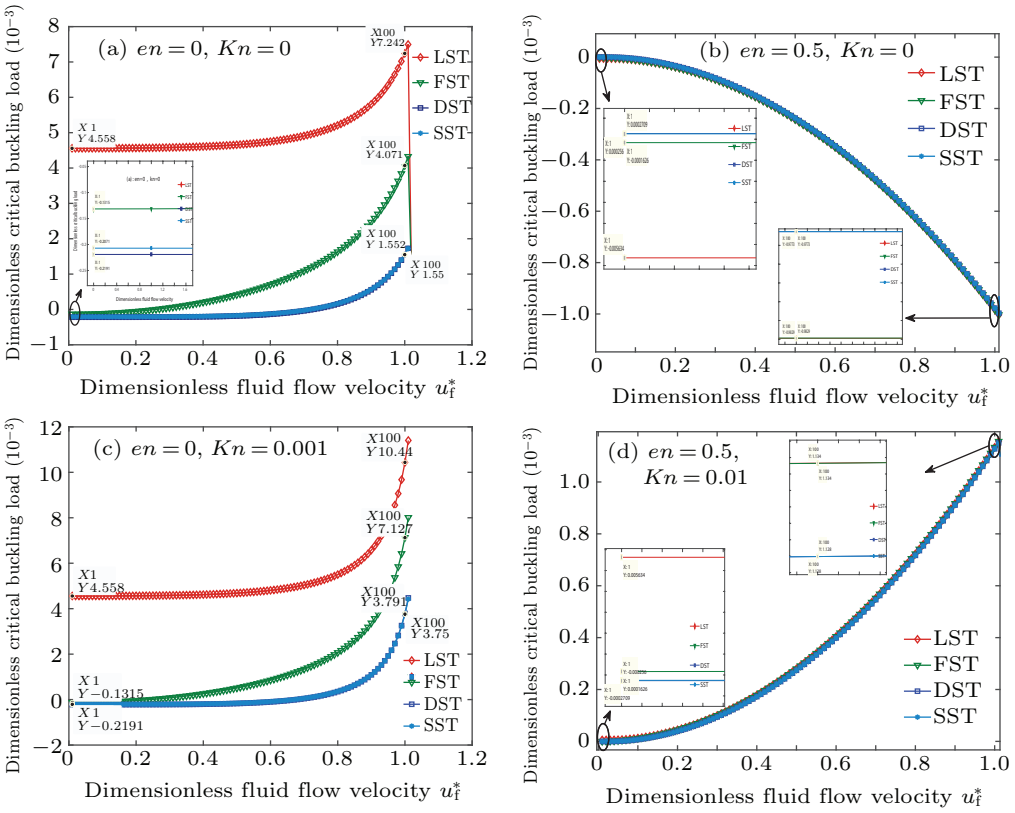


Fig. 8. Dimensionless critical buckling strain of shell cylindrical CNT against dimensionless nanofluid flow velocity considering nonlocal Love, Flügge, Donnell, and Sanders shell theories for (a) $e_n = 0$ and $Kn = 0$, (b) $e_n = 0.5$ and $Kn = 0$, (c) $e_n = 0$ and $Kn = 0.01$, (d) $e_n = 0.5$ and $Kn = 0.01$.

In Fig. 8(c), the value of the Knudsen number is assumed to be 0.01. The results show that, at the fluid velocity of zero, the critical buckling value is equal to the values obtained in Fig. 8(a) and, by applying the velocity correction factor (VCF) at a fluid velocity of 10, these values are 10.44, 7.127, 3.791, and 3.755, respectively, for the shell theories of Love, Flügge, Donnell, and Sanders. Therefore, increasing the amount of Knudsen number increases the critical amount of buckling, or in other words, increases the stability of the system.

In Fig. 8(d), the values of e_n and Kn are considered to be 0.5 and 0.01, respectively. It has been reported here that the amount of critical buckling load is reduced by increasing the nonlocal parameter [see Fig. 8(b)] and increasing with the increase of the Knudsen number [see Fig. (c)]. From Fig. 8(d), it can be observed that with a simultaneous increase of both parameters, the critical load value of the buckling increases by

increasing the flow velocity. Although this incremental trend is less than the magnitude of increase in the state a [Fig. 8(a)], it can be concluded that the effect of small-scale fluid is greater than the small-scale effect of the structure on the buckling of the system.

In addition, it can be deduced from Figs. 8(b) and 8(d) that the application of the nonlocal parameter (i.e., taking into account the effect of the nano-size scale on the structure) results in convergence of the obtained results from diverse theories.

4.5. The effect of mass density on the critical buckling strain

In this subsection, we consider the effect of the mass density of the passing fluid through the CNT on the system's critical buckling strain. To this end, water and acetone as liquid and air as gas are investigated, herein. Before using data in Tables 2 and 3, it should be noted that according to Rashidi *et al.*,[33] the range of Kn could vary from 0.001 to 0.01 for a liquid nano-flow and 0.001 to 2 for a gas nano-flow. Here, in order to compare the results, the value of the Knudsen number for all three fluids is considered to equal 0.01. In Fig. 9, the dimensionless critical buckling load variations are shown toward the increase in the fluid flow velocity. It is noticeable that in all the cases the amount of critical load increases.

It is indicated that in all the cases the value of critical buckling load increases. The ratios of this increase for distinct fluids are different so that for example at the dimensionless fluid velocity of 10, the critical loads' values of buckling are 70.3, 55.54, and 0.07944 for passing nano-water ($\rho = 1$ g·cm^{-3}), nano-acetone ($\rho = 0.79$ g·cm^{-3}), and nano-air ($\rho = 0001169$ g·cm^{-3}), respectively. Hence, it can be concluded that increasing the mass density of the passing fluid through the structure leads to an increase in the critical buckling load value. The results in this subsection are derived using the nonlocal Sanders shell theory.

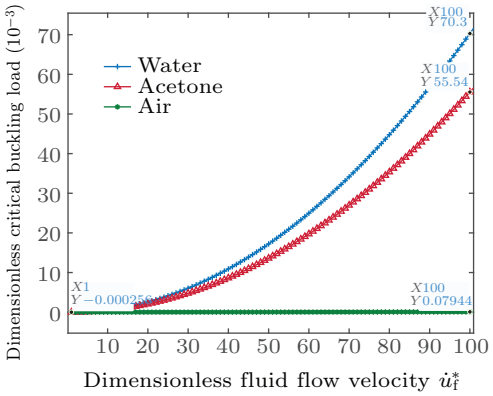


Fig. 9. Dimensionless critical buckling strain of shell cylindrical CNT against dimensionless nanofluid flow velocity considering nano-liquid of water and acetone as well as nano-gas of air.

4.6. The CNT aspect ratio effects

In this subsection, the effects of the aspect ratio of the carbon nanotube are studied by taking into account three nanotubes CNT (5,5) with $d = 6.78$ Å, CNT (7,7) with $d = 9.492$ Å, and CNT (8,8) with $d = 10.848$ Å. For verification purposes, the obtained results of the critical strain are compared with the results of the molecular simulations (MD) and the results of Refs. [20,21] in Table 9. It should be noted that the aspect ratio for the transition between shell and column behavior is given by[20]

$$\left(\frac{L}{d}\right)_t \approx 3.8\sqrt{\frac{r}{h}}. \tag{46}$$

The aspect ratios for shell-column transition are $(L/d)_t = 8.6121$, 10.190, and 10.894 using thickness $h = 0.66$ Å, half-wave numbers $m = 1$ and $n = 5$, and Knudsen number of 0.001. The results presented in Table 9 show a very good agreement for all the four nonlocal shell theories with the results of molecular simulations. As mentioned above, it is important to use the appropriate value for a nonlocal parameter to achieve acceptable results.

Table 9. Comparison between critical buckling strain of CNT (5,5), CNT (7,7), and CNT (8,8) obtained from MD simulations, Refs. [20,21][I], and proposed nonlocal Love, Flügge, Donnell, and Sanders shell cylindrical theories considering given properties[II] ($m = 1$, $n = 5$).

				Present work							
				Love shell theory		Flügge shell theory		Donnell shell theory		Sanders shell theory	
	$\left(\frac{L}{d}\right)_t$ [III]	MD	Reference data	e_0a	LST	e_0a	FST	e_0a	DST	e_0a	SST
CNT (5,5)	8.6121	0.0753	0.0818	2.67	0.0750599	1.78	0.075631	1.82	0.07510	1.74	0.07504
CNT (7,7)	10.190	0.0651	0.0613	4.15	0.0651447	2.30	0.064828	2.33	0.06537	2.24	0.06490
CNT (8,8)	10.894	0.0314	0.0311	6.59	0.0314362	3.34	0.031458	3.40	0.031415	3.49	0.031403

[I]Results of CNT (5,5) and CNT (7,7) are put from Ref. [20], and the result of CNT (8,8) is put out from Ref. [21].
[II]The considered properties are $E = 5.5 \times 10^{12}$ TPa, $h = 0.66$ Å, $\upsilon = 0.19$.
[III]Herein, the unit of measurement for $(L/d)_t$ is Angstrom (10^{-10}), and for e_0a is nanometer (10^{-9}).

Moreover, the effect of increasing the aspect ratio with and without flowing fluid on the critical buckling load is shown in Fig. 10 using the nonlocal Donnell and Sanders shell theories. In Fig. 10, it can be seen that the critical buckling load value is somewhat reduced by increasing the amount of the aspect ratio. The critical buckling loads of the carbon nanotubes conveying nanofluid with the aspect ratio of 1 are equal to 0.6309 for both SST and DST, and with the aspect ratio of 10 are equal to 0.6228 and 0.6227 using SST and DST, respectively. These results show a decrease of 1.3%, approxi-

mately. In addition, the critical buckling loads of the carbon nanotubes without passing fluid are equal to -6.264×10^{-5} and -5.796×10^{-5} for the aspect ratio of 1, and are equal to -0.005227 and -0.005689 for the aspect ratio of 10, respectively, using SST and DST. These results demonstrate a decrease of about 99%. Furthermore, it is obvious that the critical load of buckling with the presence of fluid passing through the carbon nanotube is greater than that when the fluid does not pass through the structure.

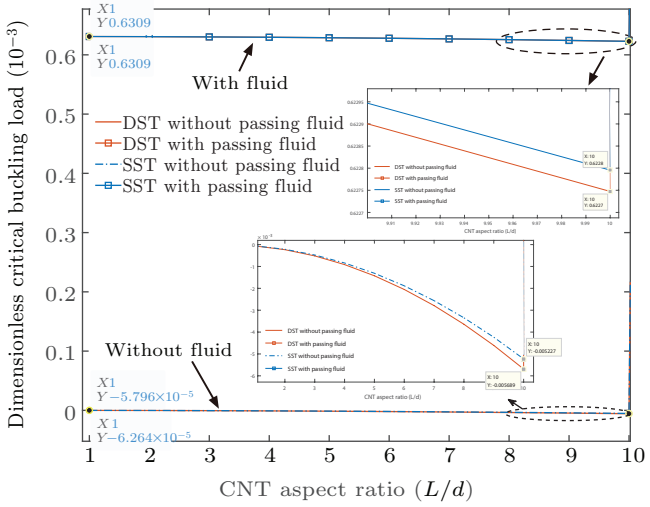


Fig. 10. Dimensionless critical buckling strain of shell cylindrical CNT against CNT aspect ratio with and without nanofluid flow utilizing nonlocal Donnell and Sanders shell theories.

4.7. Shell flexural rigidity effects

In this final subsection, we study the shell flexural rigidity effects of the CNT on the critical buckling strain value. Figure 11 demonstrates that the highest obtained amount of critical buckling load is related to the use of the nonlocal shell theories of Love, Donnell, Sander, and Flügge, respectively. It can also be seen that increasing the amount of bending rigidity of the structure causes increase in the critical buckling load.

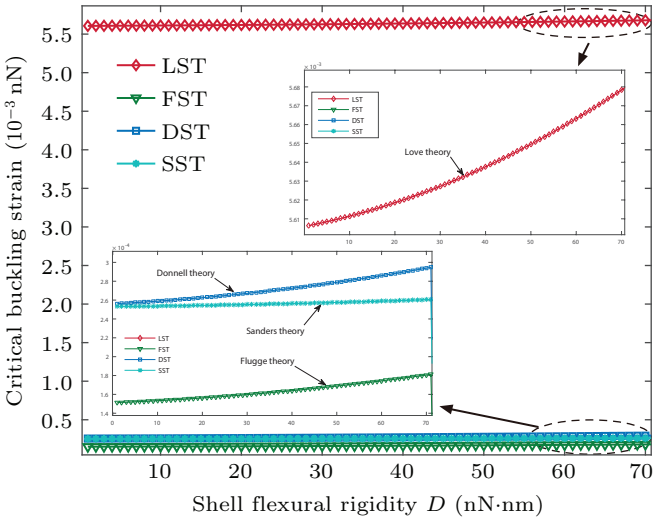


Fig. 11. Critical buckling strain of shell cylindrical CNT against shell flexural rigidity utilizing nonlocal Love, Flügge, Donnell, and Sanders shell theories.

Regarding Eq. (15) and the relationship between C_{R}, D_{R}, and G_{R}, it can be inferred that a similar incremental process is carried out by increasing the shell membrane rigidity, modulus of rigidity (shell modulus), and even the modulus of elasticity. Therefore, different values of Young's modulus used in various references[2] can play an important role in the achieved results.

5. Conclusions

In summary, we have presented the buckling behavior of CNTs embedded in simply supported ends subjected to passing nanofluid flow on the basis of the modified nonlocal Love, Flügge, Donnell, and Sanders shell theories. The governing equation containing the small-scale parameter for both structure and fluid is derived, which can be used for all four theories using different coefficients. By introducing the dimensionless parameters, the analytical solution is obtained for the dimensionless FSI governing equation in an explicit form using coding in MATLAB. In this study, it is shown that the key issue for the successful application of the nonlocal continuum mechanical models and various theories to CNT conveying nanofluid is to determine the measure and magnitude of the small-scale parameter e_0a. In most studies, e is usually taken to be 0.39 proposed by Eringen. In addition, in many articles, the small-scale parameter e_0a is found to be less than 2.0 nm for a CNT. However, there are no experiments conducted to determine the e_0a value. Moreover, it has been shown that the small-scale parameter has different values under different loading cases. Herein, the estimation of parameter e_0a is given by matching the critical buckling strain of CNT with the numerical results obtained from the molecular simulations. Moreover, the small-scale effects of the flowing fluid are investigated considering the velocity correction factor and various mass densities of nano-liquid and nano-gas. It should additionally be noted that the values of the longitudinal and circumferential half-wave numbers are also important in determining the critical load of local and general buckling and the buckling mode shapes.

Furthermore, in this study, other issues such as the effect of passing fluid and its velocity, structure aspect ratio, and shell flexural rigidity on the critical buckling strain and system stability are investigated. The results obtained from the analytical solution of the non-dimensional governing equations yielded by the Hamilton principle, taking into account all four theories, are briefly given as follows:

(i) In order to obtain the correct and precise value of the critical buckling strain, the value of the appropriate nonlocal parameter must be considered. This suitable value depends on varied conditions, such as the structural geometry (length, radius, chiral angle, etc.) and even the value of longitudinal (m), circumferential (n) half-wave number, and the buckling

mode shapes. For example, by increasing the length of the nanotubes, the value of the nonlocal parameter must also be a larger number.

(ii) In general, from $n > 5$, the critical buckling load is increased by increasing the value of n. By increasing the value of m, this value is always reduced. In addition, by increasing the number of the mode shape, the decreasing trend of the critical buckling load can be observed.

(iii) The presence of fluid through the carbon nanotubes and the increase in fluid velocity will increase the amount of critical buckling load. The highest obtained value for the critical buckling load, respectively, is related to the shell theories of Love, Flügge, Donnell, and Sanders. It can be stated that the results obtained from the sanders theory are slightly more precise according to the molecular dynamics simulations results.

(iv) Under the same conditions, increasing the nonlocal variable value and Knudsen number causes reduction and enhancement of the critical buckling strain value, respectively. By simultaneously increasing the value of the nonlocal parameter and the Knudsen number, it can be seen that the amount of critical loads will slightly increase, which means the greater effect of the small scale of the passing fluid relative to the scale of the structure. The proper choice of the nonlocal parameter value results in the convergence of the obtained results regardless of the selected shell theory and model.

(v) The critical buckling load for a structure containing a nano-liquid is greater than that when the nano-gas is passed through it. This means that increasing the fluid flow density will increase the critical buckling load and thus the system will be more stable.

(vi) By increasing the aspect ratio, flexural rigidity, shell membrane rigidity, rigidity modulus, and elasticity modulus, the buckling critical load increases.

References

[1] Craighead H G 2000 *Science* **290** 1532
[2] Kolahdoozan M, Kiani A, Heidari P and Oveissi S 2019 *Appl. Surf. Sci.* **481** 531
[3] Kolahdoozan M, Saedi H, Sina N and Oveissi S 2019 *J. Adhes. Sci. Tech.* **33** 355
[4] Oveissi S, Ghassemi A, Salehi M, Eftekhari S A and Ziaei-Rad S 2022 *Thin-Walled Struct.* **173** 108926
[5] Ai D, Qiao H, Zhang S, Luo L M, Sun C Y, Zhang S, Peng C Q, Qi Q C, Jin T Y, Zhou M and Xu X Y 2020 *Chin. Phys. B* **29** 090601
[6] Georgantzinos S K and Anifantis N K 2010 *Physica E* **42** 1795
[7] Joshi A Y, Harsha S P and Sharma S C 2010 *Physica E* **42** 2115
[8] Babu S, Ndungu P, Bradley J C, Rossi M P and Gogotsi Y 2005 *Microfluid Nanofluid* **1** 284
[9] Song X, Li B and Xie L 2020 *Chin. Phys. B* **29** 086201
[10] Wang X Y and Wang X 2004 *Compos. Part B-Eng.* **35** 79
[11] Zhou Y N and Huang G Y 2014 *Chin. Phys. Lett.* **31** 116202
[12] Oveissi S, Eftekhari S A and Toghraie D 2016 *Physica E* **83** 164
[13] Oveissi S and Ghassemi A 2018 *Appl. Math. Model.* **60** 460
[14] Iijima S 1991 *Nature* **354** 56
[15] Wang W, Deguchi Y, He Y S and Zhang J Z 2019 *Acta Phys. Sin.* **68** 234303 (in Chinese)
[16] Oveissi S, Toghraie D, Eftekhari S A and Chamkha A J 2019 *Int. J. Numer. Methods Heat Fluid Flow* **30** 1773
[17] Oveissi S, Toghraie D S and Eftekhari S A 2017 *Int. J. Fluid Mech. Res.* **44** 115
[18] Oveissi S, Toghraie D S and Eftekhari S A 2018 *Int. J. Fluid Mech. Res.* **45** 171
[19] Zhang Y Y, Wang C M, Duan W H, Xiang Y and Zong Z 2009 *Nanotechnology* **20** 395707
[20] Silvestre N, Wang C M, Zhang Y Y and Xiang Y 2011 *Composite Struct.* **93** 1683
[21] Love A E H 2013 *A treatise on the mathematical theory of elasticity* (New York: Cambridge University Press) p. 553
[22] Flügge W 2013 *Stresses in shells* (Berlin: Springer) p. 407
[23] Donnell L H 1933 *Stability of thin-walled tubes under torsion* (USA: University of North Texas Libraries) pp. 7–29
[24] Sanders J J L 1963 *Quart. Appl. Math.* **21** 21
[25] Salahshour S and Fallah F 2018 *Thin-Walled Struct.* **124** 81
[26] Arash B and Wang Q 2012 *Comput. Mater. Sci.* **51** 303
[27] Wang Q and Varadan V K 2007 *Smart Mater. Struct.* **16** 178
[28] Jaunky N and Knight Jr N F 1999 *Int. J. Solids Struct.* **36** 3799
[29] Stein M 1986 *AIAA J.* **24** 1537
[30] Paidoussis M P 1998 *Fluid-structure interactions: slender structures and axial flow* (California: Academic Press) p. 196
[31] Drazin P G and Riley N 2006 *The Navier–Stokes equations: A classification of flows and exact solutions* (New York: Cambridge University Press) p. 11
[32] Rashidi V, Mirdamadi H R and Shirani E 2012 *Comput. Mater. Sci.* **51** 347
[33] Pollard W G and Present R D 1948 *Phys. Rev.* **73** 762
[34] Kamidakis G, Beskok A and Aluru N 2005 *Microflows and nanoflows: Fundamentals and simulation* (New York: Science-Business Media) p. 51
[35] Ansari R and Rouhi H 2015 *Int. J. Nano Dimension* **6** 453 (in Persian)
[36] Loy C T and Lam K Y 1997 *Int. J. Mech. Sci.* **39** 455
[37] Pellicano F and Amabili M 2003 *Int. J. Solids Struct.* **40** 3229
[38] Hu Y G, Liew K M, Wang Q, He X Q and Yakobson B I 2008 *J. Mech. Phys. Solids* **56** 3475